Developmental, regenerative, and behavioral dynamics in acoel reproduction

Vikram Chandra[#*], Samantha E. Tseng[#†], Allison P. Kann, D. Marcela Bolaños, Mansi Srivastava*

Department of Organismic and Evolutionary Biology, Museum of Comparative Zoology, Harvard University, 52 Oxford Street, Cambridge, MA 02138

[†] Current address: The Rockefeller University, 1230 York Avenue, New York, NY 10065

# These authors contributed equally.

* Corresponding authors. Emails: vchandra1@fas.harvard.edu, mansi@oeb.harvard.edu

Abstract

Acoel worms belong to an enigmatic and understudied animal lineage in the phylum Xenacoelomorpha. Sparse taxonomic and histological work suggests that these worms exhibit a diversity of reproductive anatomies and likely a corresponding diversity in reproductive behavior. Here, we study the reproductive life history of the three-banded panther worm *Hofstenia miamia*, an acoel that is emerging as a lab-tractable model system. Using confocal microscopy and histology, we describe *H. miamia*'s reproductive organs, identifying structures previously unknown in acoels. Following a cohort of worms from zygote to adulthood, we quantify the developmental dynamics of their reproductive organs, and find that these organs emerge in a stereotyped sequence as a function of increasing body size. Studying the dynamics of organ growth and de-growth during regeneration and in starvation, we show that reproductive organs follow similar growth rules in these contexts, suggesting that they are regulated by a size-

associated program in all growth contexts. Finally, we study egg-laying behavior, finding that *H. miamia* lay their eggs through their mouths after loading them into their pharynges. Worms lay eggs for multiple months after a single mating, suggesting long-term sperm storage despite lacking a storage organ; we also find that worms can lay viable eggs without mating, indicating a capacity for self-fertilization. Further, we show that worms assess their environment to make decisions about when and where to lay their eggs, and sometimes lay eggs in communal clutches. Together, our work establishes foundational knowledge to enable the experimental study of reproductive anatomy, physiology, and behavior in acoels.

Introduction

Reproduction is critical for evolutionary success, and animals display great diversity in their reproductive life histories. The structures and strategies employed for reproduction have been relatively well-studied in some animal lineages, such as arthropods and vertebrates (Davies et al., 2013). However, a full understanding of reproductive biology is lacking in many animal phyla. For example, Phylum Xenacoelomorpha, which includes acoels, nemertodermatids, and xenoturbellids, is an early branching bilaterian lineage of primarily marine worms whose life histories are largely unknown (Cannon et al., 2016; Kapli and Telford, 2020; Philippe et al., 2011) (Fig. 1A).

Roughly 400 species of acoel worms have been described (Achatz et al., 2013; Jondelius et al., 2011; Tyler, S., Schilling, S., Hooge, M., & Bush, L. F., 2012; Wallberg, 2012). Analyses of histological sections of specimens collected in the field suggest that, with few exceptions (Crezée, 1975; Mamkaev, 1965; Raikova et al., 1995), acoels are simultaneous hermaphrodites. Unlike many marine animals that reproduce sexually through spawning and external fertilization, e.g., cnidarians, poriferans, echinoderms, etc. (Giribet and Edgecombe, 2020), acoels have been reported to reproduce sexually through internal fertilization (Achatz et

al., 2013). They exhibit a striking diversity in their reproductive anatomy (Table S1). This anatomical variation likely accompanies variation in reproductive physiology and behavior. While a few species have been cultured in the lab (Bailly et al., 2014; De Mulder et al., 2009; Shannon and Achatz, 2007; Zauchner et al., 2015), little is known about how acoels develop their reproductive organs, mate, or lay eggs.

To improve our understanding of acoel life histories, we studied reproduction in a lab tractable species, the three-banded panther worm *Hofstenia miamia* (Fig. 1B,C). *H. miamia* is a new research organism with features that allow us to study it in controlled conditions: its life cycle can be closed in the lab (worms develop from embryo to gravid adult in 2-3 months), and there is a growing array of experimental tools to observe and manipulate the worms (Gehrke et al., 2019; Hulett et al., 2023; Kimura et al., 2022, 2021; Ricci and Srivastava, 2021; Srivastava, 2022). Histology-based work has described the coarse anatomy of reproductive organs in animals in the genus *Hofstenia* (Beltagi and Mandura, 1991; Bock, 1923; Corrêa, 1960; Hooge et al., 2007; Hookabe et al., 2024; Steinböck, 1966). However, the fine structure of these organs, how they grow and develop, and how they function in the course of reproductive behavior remains unknown. To address these questions about the reproductive life history of *H. miamia*, we use a combination of light and confocal microscopy, fluorescence *in situ* hybridization, immunofluorescence, and histology, as well as observations of reproductive development and behavior in controlled conditions. We reveal new facets of acoel reproductive biology, show that active processes of growth and destruction ensure coordinated organ development and regeneration, and establish a foundation for the mechanistic study of reproduction in acoels.

Results

An overview of *Hofstenia miamia*'s reproductive anatomy

The genus *Hofstenia* (Bock, 1923) lies within the family Hofsteniidae. The family currently contains four genera (Ahyong et al., 2024; Hookabe et al., 2024) and is an early-branching lineage within acoels (Abalde and Jondelius, 2024; Jondelius et al., 2011). Three species are currently recognized within the genus *Hofstenia*: *H. atroviridis*, *H. miamia*, and *H. arabiensis* (Ahyong et al., 2024; Beltagi and Mandura, 1991; Bock, 1923; Corrêa, 1960; Hooge et al., 2007). Like other acoels, *Hofstenia* are considered to be simultaneous hermaphrodites (Beltagi and Mandura, 1991; Bock, 1923; Corrêa, 1960; Hooge et al., 2007; Steinböck, 1966).. *Hofstenia miamia* is likely the most common and widespread species within the genus, with a geographic distribution in the Caribbean and the North Atlantic, including the Bahamas and the Florida coast (Beltagi and Mandura, 1991; Bock, 1923; Corrêa, 1960; Hooge et al., 2007; Steinböck, 1966). All three *Hofstenia* species are described as having an anterior male reproductive system including a seminal vesicle, prostatic vesicle, a penis with sclerotized needles, 'diffuse' testes, and a ventral male gonopore near the mouth (Beltagi and Mandura, 1991; Bock, 1923; Corrêa, 1960; Hooge et al., 2007; Steinböck, 1966). The female reproductive system, as described, includes two ovaries spanning the posterior two-thirds of the worm. However, these descriptions were all based on worms roughly 5-8mm in length (Beltagi and Mandura, 1991; Bock, 1923; Corrêa, 1960; Hooge et al., 2007; Steinböck, 1966). In our lab cultures, fully grown adult *H. miamia* can be over 1.4cm in length. We noticed that these large adults were more likely to reproduce than smaller worms, and we reasoned that their anatomy could also be different. We therefore began by re-examining the coarse anatomy of *Hofstenia miamia*.

We anesthetized adult worms, mounted them ventral side up on a slide, and imaged them through a dissecting microscope and found, as expected, that *H. miamia*'s male

100 copulatory structures are located in the anterior of the animal, just posterior to the mouth (Fig.
101 1C,D; Fig. S1A). These male structures are located within a translucent cylindrical region close
102 to the ventral surface of the worm and immediately ventral to the pharynx. We observed two
103 opaque, white regions within the male copulatory apparatus, located towards its posterior (Fig.
104 1C; Fig. S1A). The larger, posterior oval structure corresponds to the seminal vesicle, while the
105 smaller, teardrop-shaped anterior structure corresponds to the prostatic vesicle (Fig. 1C,D; Fig.
106 S1A) (Beltagi and Mandura, 1991; Bock, 1923; Corrêa, 1960; Hooge et al., 2007; Steinböck,
107 1966). Previous work reported that *H. miamia* has a penis (Fig. S1A): a sperm-delivery organ
108 containing rigid needles known as 'stylets' (Hooge et al., 2007; Steinböck, 1966). Although
109 stylets are difficult to see in this imaging preparation, we identified a small aperture immediately
110 posterior and ventral to the mouth (Fig. S1A), and we observed that the worm extended its
111 penis through it, showing that this aperture is the male gonopore and confirming the location of
112 the penis in the anterior of the worm.
113 As previously described (Beltagi and Mandura, 1991; Bock, 1923; Corrêa, 1960; Hooge
114 et al., 2007; Steinböck, 1966), we found that the female reproductive system occupies the
115 posterior two-thirds of the worm (Fig. 1C,D; Fig. S1B). This system consists of numerous eggs
116 grouped into three distinct clusters: one lateral group on each side of the body extends along
117 the anterior-posterior axis (Fig. S1B) and a medially-located cluster present just posterior to the
118 pharynx (Fig. S1C). The lateral clusters contain oocytes of various sizes, likely corresponding to
119 different stages of maturation. These oocyte-laden regions in the parenchyma have been
120 identified as the ovaries in historical reports (Beltagi and Mandura, 1991; Bock, 1923; Corrêa,
121 1960; Hooge et al., 2007; Steinböck, 1966). Within the ovaries, there is no obvious organization
122 of oocytes (by size or shape) along any of the worm's body axes. All oocytes within the ovaries
123 have a germinal vesicle, a nucleus arrested in prophase I of meiosis that is a common feature of
124 oocytes of nearly all animals (Grossman et al., 2017; Herlands and Maul, 1994; Liu et al., 2006;
125 Munro et al., 2023). This nucleus breaks down during early oogenesis or after fertilization

126 (Falleni and Gremigni, 1990; Sagata, 1996), suggesting that *Hofstenia*'s lateral oocytes are
127 likely unfertilized.
128 Posterior to the pharynx, there is often a cluster of uniformly sized, spherical eggs that
129 do not have a germinal vesicle (Fig. 1C,D; Fig. S1C). The number of eggs at this position is
130 highly variable, ranging from zero to over a dozen eggs. In *H. atroviridis*, Bock (Bock, 1923)
131 speculated that these eggs are mature, fertilized, and ready to be laid: i.e., zygotes. To test
132 whether these eggs were indeed zygotes, we dissected out eggs from this midline cluster, as
133 well as from the lateral ovaries. We found that 46/56 eggs (removed from the midline clusters of
134 9 worms) developed and hatched into juvenile worms, in line with previously established
135 developmental timing (Fig. S1D) (Kimura et al., 2021). Meanwhile, all eggs dissected from the
136 lateral ovaries disintegrated within 48 hours. The eggs in this medial cluster are therefore
137 mature, likely fertilized, and ready for laying, while eggs in the ovaries are immature or
138 unfertilized. Overall, these observations confirm and extend previous descriptions of *H. miamia*,
139 and provide a high-level overview of its reproductive anatomy. Next, taking advantage of *H.*
140 *miamia*'s tractability, we sought to obtain a finer understanding of its reproductive structures and
141 their development.
142
143
144 **Dynamics of reproductive organ development**
145 How reproductive structures develop as animals reach sexual maturity is not well understood in
146 the Xenacoelomorpha. As in the acoel *Aphanostoma pulchra* (previously *Isodiametra pulchra*)
147 (Chiodin et al., 2013), hatchling *H. miamia* have no visible reproductive structures, and previous
148 observations suggested that these develop over a month after hatching as the worms grow
149 toward adulthood (Kimura et al., 2021; Srivastava, 2022). To determine the timeline and
150 dynamics of reproductive development, we reared 42 zygotes in isolation and monitored their
151 growth over time (Fig. 1E,F), precisely controlling their rearing environment such that each

152 animal had access to controlled amounts of seawater and food (see Methods). To assess
153 whether nutrition affects reproductive development, we split the cohort of hatchling worms into
154 two groups that were fed differently. For each group, we gradually increased the amount of food
155 they were given as they grew larger, to ensure that worms always had *ad libitum* food access
156 while avoiding unnecessary overfeeding. These food increases occurred periodically, but we
157 delayed them by two weeks for one feeding group (Fig. S2A,B). We reasoned that this
158 treatment would delay growth in one group, allowing us to decouple biological age from organ
159 and body growth. Twice weekly, we captured images of the ventral surface of each worm and
160 quantified the size of each visible reproductive structure.

161 We found that worms maintained their aspect ratio from hatchling to adult, growing
162 proportionally over time (Fig. 1E-H; Fig. S2C). At every stage of development, the size of each
163 reproductive organ scaled with body size once that organ appeared (Fig. 1I-K). Worms with
164 delayed increases in feeding displayed corresponding delays in their growth, both in their body
165 size (Fig. S2D) and in the timing of appearance of their ovary and seminal vesicle (Fig. 1L). The
166 penis and seminal vesicle developed at a smaller size in these worms compared to worms
167 without delayed feeding increases (Fig. 1M), suggesting that resource-limited worms may invest
168 disproportionately in male development. Multiple regression found that organ size was
169 explained by both age and body size, but that body size was a better predictor of the size of
170 each reproductive organ (Table S2). This suggests that the differentiation and growth of
171 reproductive structures is coupled to the worm's body size, rather than to its age.

172 We found that reproductive development generally occurs in a stepwise fashion, where
173 organs appear in a consistent sequence at serially increasing body sizes. Newly hatched
174 animals possess all major somatic organs (such as a brain, muscle system, pharynx, gut, etc.
175 (Kimura et al., 2022, 2021)), but lack all reproductive structures (Fig. 1E,F). 4-6 weeks after egg
176 laying, when the worm is about 3 ± 0.6 mm (mean ± SD) in length, the anterior-ventral tissue
177 housing the future male copulatory apparatus becomes visibly less dense, and a groove

178 becomes apparent in the ventral surface. Soon after, the male gonopore becomes detectable
179 posterior to the mouth. Sperm begin to accumulate in the seminal vesicle around 35 days post
180 laying, once a worm is about 4.4 ± 0.9 mm (mean ± SD) long. Shortly after, when a worm is 5.6
181 ± 0.9 mm (mean ± SD), the first oocytes become visible in nascent ovaries. These ovaries grow
182 with the worm over time, with existing oocytes maturing and new ones continuously added.
183 Around two months after being laid, typically after a worm is 8.7 ± 1.2 mm in length, eggs
184 appear near the base of the pharynx (Fig. 1E,F,L,M). These eggs are laid within hours or days,
185 and they develop and hatch into juvenile worms. Given that these worms were isolated since
186 birth, this suggests that *H. miamia* can reproduce through self-fertilization.
187 To visualize the extent to which reproductive structures develop in sequence, we ranked
188 each structure in each worm by its date of appearance (Fig. 1N). All worms, without exception,
189 first developed a penis. A few worms simultaneously developed a seminal vesicle; in most other
190 worms, this structure appeared second, with a few developing their seminal vesicle concurrent
191 with nascent ovaries. Ovaries always appeared before the first fertilized eggs were seen in the
192 central region. Next, we asked whether the left and right ovaries of each worm developed in
193 synchrony. We found that on the first day that an ovary was visible, 34/34 worms had both
194 ovaries visible. Partial regression analysis revealed that the sizes of the two ovaries within a
195 worm are strongly correlated, even when correcting for body size (Fig. S2E). Consistent with
196 findings from many other bilaterally-symmetric organs (Allard and Tabin, 2009; Boulan and
197 Léopold, 2021; Harris et al., 2021; Vallejo et al., 2015; Wolpert, 2010), this suggests that an
198 active process may synchronize ovarian growth within individual worms.
199

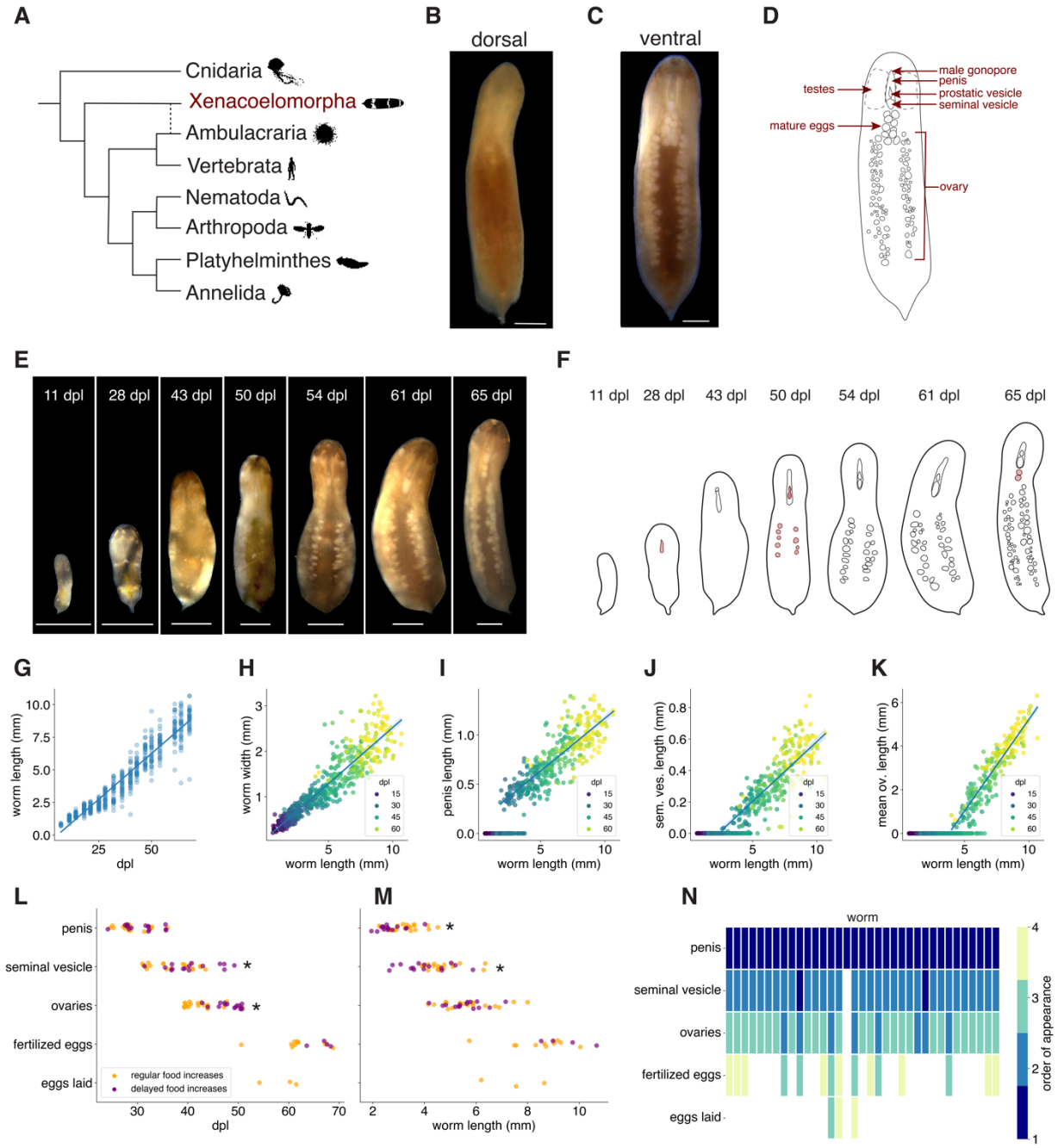

Figure 1: Reproductive organs develop sequentially following scaling rules. (**A**) Xenacoelomorpha is an early-branching bilaterian lineage of aquatic worms. Phylogeny modified from (Srivastava, 2022). Animal icons are from phylopic.org, and are in the public domain; the dashed line reflects uncertainty in the consensus phylogeny (Cannon et al., 2016; Kapli and Telford, 2020; Philippe et al., 2011). (**B**) Dorsal view of an adult *Hofstenia miamia*. (**C**) Ventral view of an adult *Hofstenia miamia*; most reproductive structures are visible in this view. (**D**) Schematized view of the ventral surface of a worm with known

207 reproductive structures illustrated. (**E**) Timecourse of a representative worm through development, from
208 hatchling to reproductively mature adult. (**F**) Schematic of timecourse shown in (**E**) with key reproductive
209 developments illustrated. The first appearance of each organ is highlighted in red. (**G**) The length of
210 worms increases over time ($R^2 = 0.91$, $p < 0.0001$), and (**H**) worms grow proportionally: their length scales
211 with their width ($R^2 = 0.85$, $p < 0.0001$). Error band shows 95% confidence interval. (**I-K**) The length of
212 each reproductive organ scales with increases in body size (penis: $R^2 = 0.70$, $p < 0.0001$; seminal vesicle:
213 $R^2 = 0.63$, $p < 0.0001$; ovaries: $R^2 = 0.84$, $p < 0.0001$). Error band shows 95% confidence interval, with
214 zero values excluded from these regressions. (**L**) Worms with delayed feeding increases had significant
215 delays in the appearance of their seminal vesicle and ovaries, but not the penis (Welch's t test for date of
216 appearance for penis: $p = 0.08$, seminal vesicle: $p = 0.04$, ovary: $p < 0.0001$; $n \geq 15$). (**M**) Worms with
217 delayed feeding increases had a smaller body length when a penis and seminal vesicle appeared, but not
218 when ovaries appeared (Welch's t test for length on date of appearance for penis: $p = 0.005$, seminal
219 vesicle: $p = 0.03$, ovary: $p = 0.74$; $n \geq 15$). Asterisks indicate statistical significance. (**N**) Ranking the order
220 in which reproductive organs appear (y-axis) in developing worms reveals a stepwise pattern of
221 reproductive differentiation. The x-axis shows individual worms. dpl = days post laying. Scale bars: 1 mm.
222

223 **De-growth and regeneration of reproductive organs**

224 Next, we asked whether these patterns of growth persisted in different contexts. *H. miamia*, like
225 other studied acoels, is an excellent regenerator and can regenerate all tissues from a wide
226 range of initial tissue configurations (Srivastava, 2022; Srivastava et al., 2014; Steinböck, 1966).
227 We amputated and followed adult worms in three ways: by isolating tail tips (which contain no
228 reproductive structures) and studying how they regenerated the majority of their organs, by
229 cutting worms sagittally and studying how they regenerated their missing half, and by isolating
230 heads from tails and studying how these head fragments regenerated their tails and the
231 posterior region of their ovaries (Fig. 2A). Head and tail fragments both gradually increased in
232 size, with tail fragments growing much faster in size (Fig. S3A-G). Within two weeks, most of

233 these fragments had regained the characteristic shape of intact worms. Sagittally-cut fragments
234 first shrank in size before subsequently growing (Fig. S3G), and appeared to take longer to fully
235 regain normal worm-like appearance (Fig. S3C,D). All reproductive organs gradually
236 regenerated, with growth dynamics contingent on the nature of the injury (Fig. 2B-J; Fig. S3A-
237 F,H,I). Additionally, we asked how reproductive organs change in another context: degrowth.
238 Anecdotal observations suggested *H. miamia* tolerates long periods of starvation but gradually
239 shrinks in size when deprived of food. We used this starvation-induced de-growth to ask
240 whether reproductive organs scale with decreasing body size. We starved a cohort of adult
241 worms and quantified the de-growth of their reproductive organs over time (Fig. 2K,L). We found
242 that all worms survived over three months of continuous starvation, gradually shrinking over
243 time (Fig. 2M). Worms maintained their aspect ratios as they shrank (Fig. 2K,L,N), and their
244 reproductive organs shrank correspondingly (Fig. S4A-E). Partial regression analysis of
245 shrinking ovaries showed that they shrink synchronously (Fig. S4F), suggesting active
246 coordination of de-growth across the left-right axis.
247 The stepwise growth relationships we found between reproductive organs and body size
248 during post-embryonic development largely generalized to both regeneration and de-growth
249 (Fig. S4G-I). Starving worms lost most reproductive organs in the opposite order to which they
250 developed them, first losing fertilized eggs, then ovaries, and eventually losing their seminal
251 vesicle (Fig. 2O,P). However, after three months of starvation, most worms continued to retain
252 their penes despite being below the threshold size at which we would expect to see loss of this
253 organ (Fig. 2O), perhaps because rigid, sclerotized structures degrade differently from soft
254 tissue. In regenerating tail fragments, the male reproductive structures generally developed
255 before the female reproductive structures, following similar stepwise patterns to developing
256 juvenile worms (Fig. 2Q). Scaling coefficients for each organ were statistically distinguishable
257 across development, regeneration, and de-growth, but the effect sizes of the differences
258 between coefficients were generally small (Fig. S4G-I, Table S3). Analyzing this effect in more

detail, we found that unsurprisingly, amputated worms initially display aberrant organ scaling but recover typical scaling as they regenerate (Fig. S4J-L). Qualitatively, across all of these growth contexts, reproductive organs scaled with body size in similar ways (Fig. S4G-I, Table S3).

In sagittally-cut worms, each worm fragment retained one of its two ovaries immediately after amputation. These ovaries first partially degenerated before growing back (Fig. 2G; Fig. S3C,D), consistent with the reported loss of germline tissue during early regeneration in heads regrowing tails (Hulett et al., 2023). Body size also decreased after sagittal amputation (Fig. S3G), but ovarian degrowth was disproportionate (Fig. S4M). The rate of ovarian degrowth (normalized to body size) was significantly greater than the rate of normalized ovarian degrowth during starvation (Fig. S4M). Consistent with studies showing extensive cell death during early regeneration in other systems (Ballarin et al., 2008; Pellettieri et al., 2010; Rychel and Swalla, 2008), this suggests that an active destructive process is responsible for degrowth during ovary regeneration in acoels. The missing ovary began to grow back roughly one month after amputation. We found that the ovaries grew asymmetrically in these worms, with the new ovary growing faster (Fig. 2G). This suggests the existence of an active growth mechanism to ensure that both ovaries reach a symmetric target size.

Together, our results suggest the existence of a size-associated program that regulates the development of reproductive organs, as well as active tissue growth and destruction mechanisms to achieve organ symmetry. It is likely that this program regulates reproductive organ growth in a variety of different developmental contexts, including the transition from juvenile to adult worm, regeneration after injury and tissue loss, and during starvation-induced de-growth. With this high-level understanding of male and female reproductive system anatomy and the scaling relationships that govern their formation in hand, we next sought to understand these systems at higher resolution in order to decipher their functional morphology.

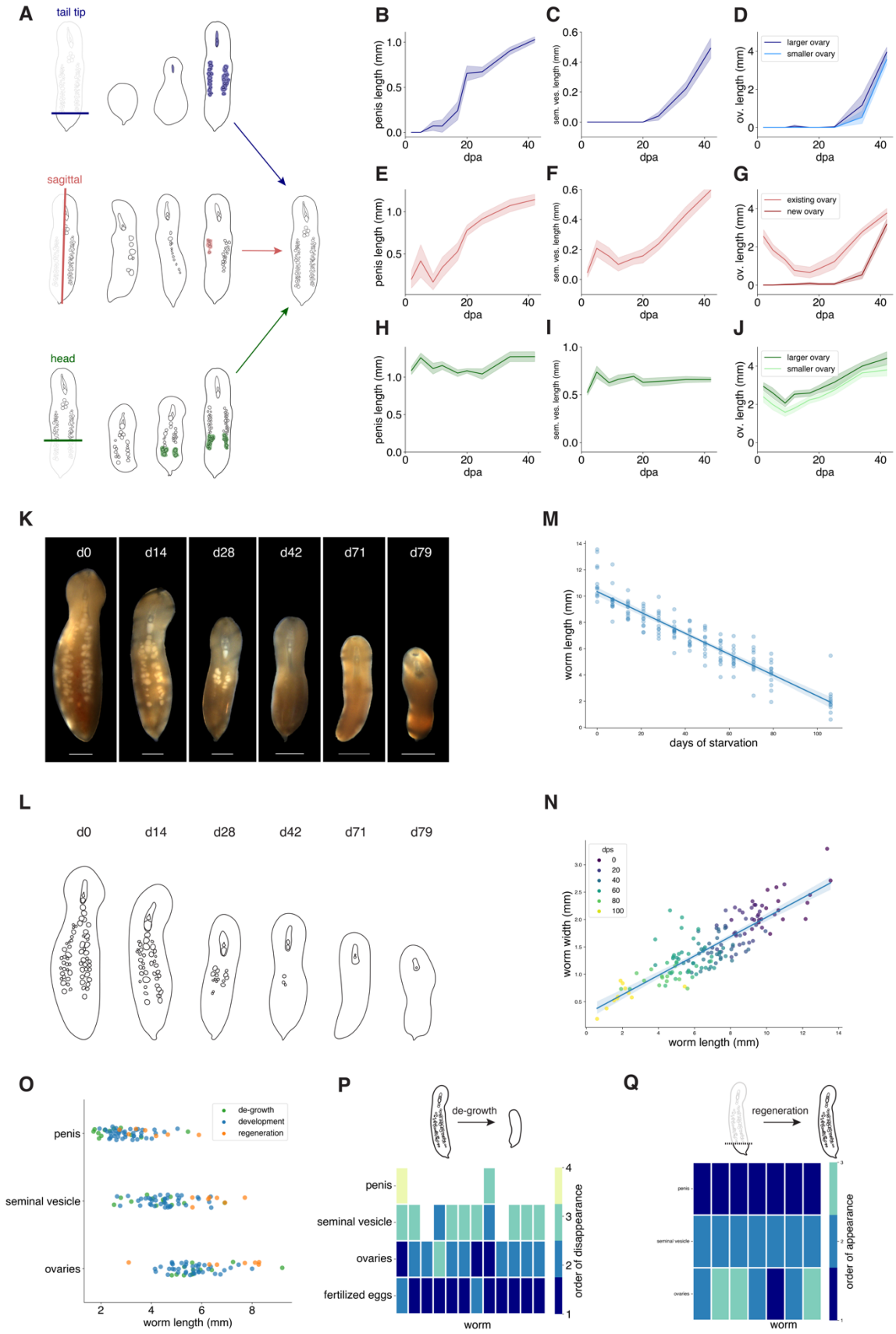
A
tail tip
sagittal
head
B
penis length (mm)
dpa
C
sem. ves. length (mm)
dpa
D
larger ovary
smaller ovary
ov. length (mm)
dpa
E
penis length (mm)
dpa
F
sem. ves. length (mm)
dpa
G
existing ovary
new ovary
ov. length (mm)
dpa
H
penis length (mm)
dpa
I
sem. ves. length (mm)
dpa
J
larger ovary
smaller ovary
ov. length (mm)
dpa
K
d0
d14
d28
d42
d71
d79
M
worm length (mm)
days of starvation
L
d0
d14
d28
d42
d71
d79
N
dps
0
20
40
60
80
100
worm width (mm)
worm length (mm)
O
de-growth
development
regeneration
penis
seminal vesicle
ovaries
worm length (mm)
P
de-growth
penis
seminal vesicle
ovaries
fertilized eggs
order of disappearance
worm
Q
regeneration
penis
seminal vesicle
ovaries
order of appearance
worm

285 **Figure 2: Reproductive organ development follows similar patterns in different growth contexts.**
286 (**A**) Schematic of regeneration of the penis, seminal vesicle, and ovaries following three different
287 amputations. Shading indicates the tissue that regenerates. (**B-J**) Growth dynamics of reproductive
288 organs (within column) for each of three amputations (within row). Error bands show SEM. (**K**) Time
289 course of a starving worm undergoing de-growth and step-wise loss of reproductive organs. (**L**)
290 Schematic of reproductive organ degradation as seen in (**K**) over the course of starvation-induced de-
291 growth. (**M**) Worm length decreases over the course of degrowth ($R^2 = 0.85$, $p < 0.0001$). Error band
292 shows 95% confidence interval. (**N**) Worms shrink as they grow; their lengths and widths decrease
293 proportionally ($R^2 = 0.73$, $p < 0.0001$). Error band shows 95% confidence interval. (**O**) Across different
294 growth contexts, reproductive organs appear or disappear at roughly consistent body lengths. Ranking
295 the order in which reproductive structures are gained in regenerating worms (**Q**) and lost in worms
296 undergoing de-growth (**P**) shows that organs are gained and lost in roughly the same order in all growth
297 contexts. The x-axis shows individual worms in these plots. dps = days post onset of starvation. dpa =
298 days post amputation. Scale bars: 1 mm.
299
300
301 **Fine structure of the male reproductive system**
302 Next, to understand the organization of male reproductive structures at high resolution, we
303 visualized them using a combination of histology, immunofluorescence, staining with live dyes,
304 and fluorescence *in situ* hybridization (FISH) (Fig. 3; Fig. S5A). The most anterior part of the
305 male copulatory apparatus is the penis. This structure is difficult to visualize under reflected
306 white illumination (Fig. 1C; Fig. S1A), but can be seen when worms extend it, which we have
307 observed them do both spontaneously and during mating (data not shown). Staining fixed
308 worms with the dye SiR-actin labels the structure clearly, and can be visualized well in smaller
309 adult worms more amenable to confocal microscopy, enabling a high-resolution view of the
310 structure (Fig. 3A-C). Components of the penis can also be seen clearly in histological sections
311 of adult worms (Fig. 3D). These show that the penis contains a bundle of rigid needle-like

312 structures (referred to as stylets) (Fig. 3E-G, Fig. S5B,C). Our observations of the stylets match
313 the description of sclerotized needles described in other species in the genus and in other
314 studies of *Hofstenia miamia* (Beltagi and Mandura, 1991; Bock, 1923; Corrêa, 1960; Hooge et
315 al., 2007; Steinböck, 1966). The stylets are situated immediately posterior to the base of the
316 penis sheath – a long, conical structure (Fig. 3C; Fig. S5E,F; Video 1). The cavity inside this
317 sheath has previously been referred to as the 'male antrum' (Beltagi and Mandura, 1991; Bock,
318 1923; Corrêa, 1960; Hooge et al., 2007; Steinböck, 1966). The base of the sheath is cup-
319 shaped, and is lined with posterior-facing hair-like extensions (Fig. 3G). At its anterior end, it
320 connects to the male gonopore (Fig. 3C). Both the gonopore and the sheath are lined with cilia
321 (Video 1,2), consistent with reports in other hofsteniid species (Beltagi and Mandura, 1991;
322 Bock, 1923; Corrêa, 1960; Hooge et al., 2007; Steinböck, 1966). During mating, the penis
323 stylets are likely pushed anteriorly, through the sheath and out of the male gonopore. This could
324 evert the sheath, resulting in a penis-extension state in which the sheath emerges through the
325 gonopore around the stylets, with the ring of protrusions now near the anterior tip of the penis. It
326 is possible that these protrusions have a sensory function, and could inform fine penis
327 movements during mating. Immunofluorescence with an antibody against FMRFamide (see
328 Methods) revealed a set of cells that resemble neurons encircling the base of the sheath (Fig.
329 S5E). Further studies will be needed to understand how these components regulate copulatory
330 behavior.

331 Next, we focused on the teardrop-shaped prostatic vesicle, which is situated anterior to
332 the seminal vesicle (Fig. 1C,D) and immediately posterior to the penis stylets (Fig. 3H,I). Our
333 histological studies show that the prostatic vesicle (Fig. S6C-E) is surrounded by glands (Fig.
334 S6F-H). The secretions of this organ are thought to mix with the sperm as it passes through
335 (Faubel, 1983; Hyman, 1951). Unexpectedly, our immunofluorescence experiments also
336 revealed a layer of cells enclosing the prostatic vesicle (Fig. 3I). This layer may be an epithelial

337 tissue most likely associated with the prostatic glands. The interior of the prostatic vesicle
338 contains densely-packed sperm cells (Fig. 3D,I; Fig. S6C-G).
339 The seminal vesicle is the posterior-most organ of the male copulatory apparatus (Fig.
340 3J). Histological staining as well as immunofluorescence staining of the muscle marker
341 Tropomyosin, showed that the seminal vesicle and prostatic vesicle are both encircled by layers
342 of muscle (Fig. S5F; Fig. S6C-H), consistent with previous descriptions (Beltagi and Mandura,
343 1991; Bock, 1923; Corrêa, 1960; Steinböck, 1966). Histological and nuclear staining of the
344 seminal vesicle in adult worms (Fig. 3J-L; Fig. S5F; Fig. S6G,H) reveal that it consists primarily
345 of sperm cells. To confirm this, we dissected the seminal vesicle out of adult worms, and stained
346 it with a nuclear dye. We found that individual cells emerged from the structure over time, and
347 high-magnification imaging showed that they were indeed sperm cells, each with a ~23μm-long
348 nucleus and a ~22μm-long flagellum (Fig. 3M). During one mating event, we observed a failed
349 attempt at insemination by a worm that resulted in the release of a packet of sperm outside its
350 partner. We recovered this 0.6 mm-long packet of sperm (Fig. S5G) and found that it consisted
351 of cells with the same morphology as those in the seminal vesicle (Fig. S5H), confirming that
352 these are indeed sperm. As an aside, acoel sperm has historically been described as
353 “biflagellate”, intended to mean that sperm cells each contain two axonemes, and this property
354 is thought to be a defining synapomorphic character of acoels (Achatz et al., 2013; Petrov et al.,
355 2004). We show that *H. miamia* sperm have a single flagellum, and suggest that the axonemal
356 properties of the flagellum may be a more accurate taxonomic character than the external
357 flagellar morphology.
358 Next, we sought to identify the testes (the organs of sperm production). Consistent with
359 previous observations (Beltagi and Mandura, 1991; Bock, 1923; Corrêa, 1960; Hooge et al.,
360 2007; Steinböck, 1966), nuclear staining and histological studies of adult worms revealed dense
361 clusters of sperm in the anterior parenchyma, wrapping around the worm’s pharynx (Fig. 3N-U).
362 Tropomyosin labeling showed that the testes are embedded within layers of muscle (Fig. S5I,J).

363 Next, inspecting germline markers identified in previous single-cell RNA sequencing data (Hulett
364 et al., 2023), we identified one likely to label testes: the gene *pa1b3-2*. FISH for *pa1b3-2* reveals
365 that this gene does indeed specifically label testes, and that its expression coincides well with
366 the dense cellular clusters visible through nuclear staining (Fig. S7A,B).

367 Finally, we studied the development of the male reproductive system, using confocal
368 microscopy to visualize the maturation of its components at high resolution. Hatchling worms do
369 not possess any visible reproductive structures. Actin staining reveals that, within the copulatory
370 apparatus, the sheath and stylets emerge first, followed by a gradually-inflating prostatic vesicle
371 (Fig. 4A). The hair-like extensions of the sheath grow and become more conspicuous over time
372 (Fig. 4A). Next, we used two methods to visualize testes maturation. First, reasoning that
373 nuclear staining may not allow us to visualize testes at the earliest developmental stages, we
374 performed FISH to detect mRNA for *pa1b3-2* in juvenile worms of various sizes. In the smallest
375 worms (i.e. ~<2 mm), there was no expression (Fig. 4B-C). In larger, reproductively immature
376 worms, we detected expression of *pa1b3-2* in two lateral clusters that expanded slightly along
377 the anterior-posterior axis as development progressed (Fig. 4B-C). Since adult testes are a
378 single cylindrical structure that wraps around the pharynx, this early developmental pattern
379 suggests that the two lateral structures must grow along the dorso-ventral and medio-lateral
380 axes until they meet in the middle. Second, to test this hypothesis, we performed nuclear
381 staining on transverse sections of worms across a broader section of development (Fig. 4D; Fig.
382 S7C). In small worms, the testes are lateralized and do not meet on the dorsal surface. In larger
383 worms, these lateral regions have expanded across the dorsal surface of the worm to form a
384 single apparently-continuous region (Fig. 4E). Many acoel species are thought to have paired,
385 lateral testes (Table S1), a feature of taxonomic importance (Jondelius et al., 2011). While
386 juvenile *H. miamia* have paired testes, these organs morph into a single cylindrical structure in
387 the transition to adulthood. As lab-reared worms can be substantially larger than those found in

388 the wild, these results raise the possibility that other acoels may undergo similar morphological
389 changes during development.
390 Together, our data provide a high-resolution view of *H. miamia's* elaborate male
391 reproductive morphology. Consistent with our quantitative data, we find that this morphology
392 emerges in a stereotyped developmental sequence during the transition to adulthood in which
393 the penis sheath develops first, followed by nascent testes, the stylets, and the membrane-like
394 structure enveloping the prostatic vesicle. Sperm presumably from the testes then travels to the
395 prostatic vesicle. Over time, as all structures grow, the hair-like projections on the back of the
396 sheath become more prominent, the testes extend both along the anterior-posterior axis and
397 dorsally to wrap around the head, and sperm cells fill the seminal vesicle. The prostatic and
398 seminal vesicles appear to be surrounded by muscle, epithelia, and gland cells. Our histological
399 sections suggest that at least in adult worms, sperm cells may enter through the posterior of the
400 seminal vesicle and travel forwards into the prostatic vesicle. We do not yet understand how this
401 occurs in juvenile worms, how sperm cells navigate to these vesicles from their varied points of
402 origin, or how they are hypodermically injected during mating.
403

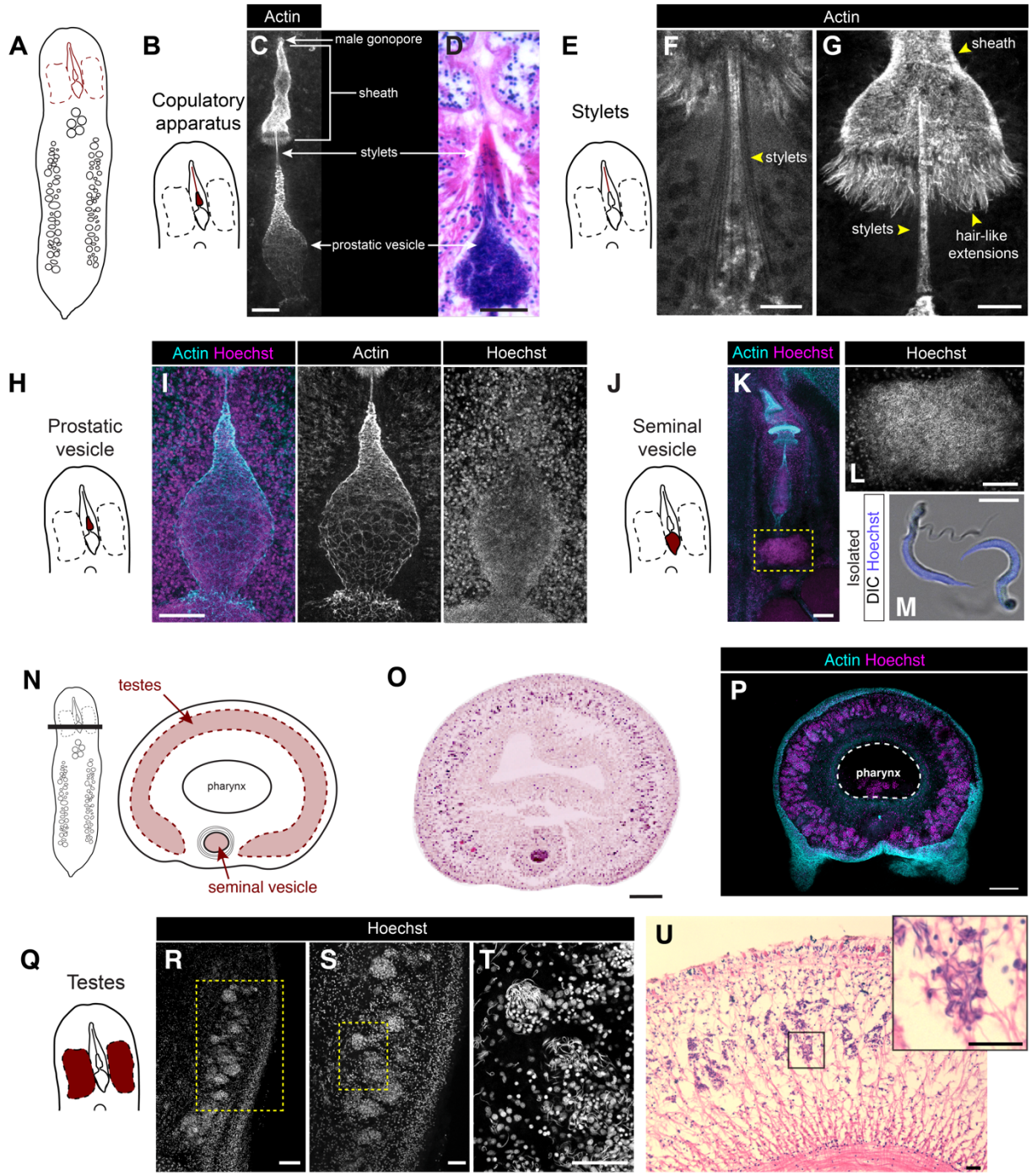

Figure 3: The male reproductive system of *Hofstenia* includes a penis with a collection of needles, a sperm containing organ (seminal vesicle), and two testes that span the dorsal surface. (**A**) A schematized view of the ventral surface of the worm with male reproductive structures highlighted in red. (**B**) Schematic of male reproductive structures with the copulatory apparatus (excluding the seminal vesicle) highlighted. (**C**) Labeling with an actin dye (white) labels the male gonopore, sheath, penis

410 stylets, and prostatic vesicle. (**D**) A histological section also reveals these organs. (**E**) Schematic of the
411 male reproductive system, with the penis stylets highlighted. (**F**) The stylets are a bundle of needles
412 labeled by actin. (**G**) The posterior of the penis sheath terminates in a ring of hair-like projections, also
413 labeled by actin. (**H**) Schematic of the male copulatory apparatus, with the prostatic vesicle highlighted. (**I**)
414 Actin staining with a nuclear label (Hoechst) shows that the prostatic vesicle is enveloped by a thin
415 epithelium-like layer, and contains densely packed sperm. (**J**) Schematic of the male copulatory
416 apparatus, with the seminal vesicle highlighted. (**K**) The morphology of the copulatory apparatus in
417 mature, adult worms is similar to that of early adults (previous panels). (**L**) The seminal vesicle of this
418 adult worm contains densely-packed sperm. (**M**) Dissecting out an adult seminal vesicle allows labeling of
419 individual sperm cells, showing their distinctive morphology. (**N**) Schematic of a transverse view of an
420 adult worm's anterior, showing the relative organization of the seminal vesicle and testes. (**O**) Transverse
421 sections show that testes appear as a continuous structure that spans the dorsal surface of the worm. (**P**)
422 The testes extend through the dorso-ventral axis of the worm and wrap around the head. The pharynx
423 (labeled and circled with a dotted line) contains residual food. (**Q**) Schematic of the male copulatory
424 apparatus, with the testes highlighted. (**R-T**) Nuclear staining on an adult worm, cut sagittally, reveals the
425 testes, which contains dense bundles of sperm organized around clusters of cells in the parenchyma. (**U**)
426 Histological sections confirm this organization of the testes. Scale bars: 20μm (C, U), 10μm (F-G, M),
427 50μm (D,I,S, T), 100μm (K,L,R), 200μm (O, P).
428

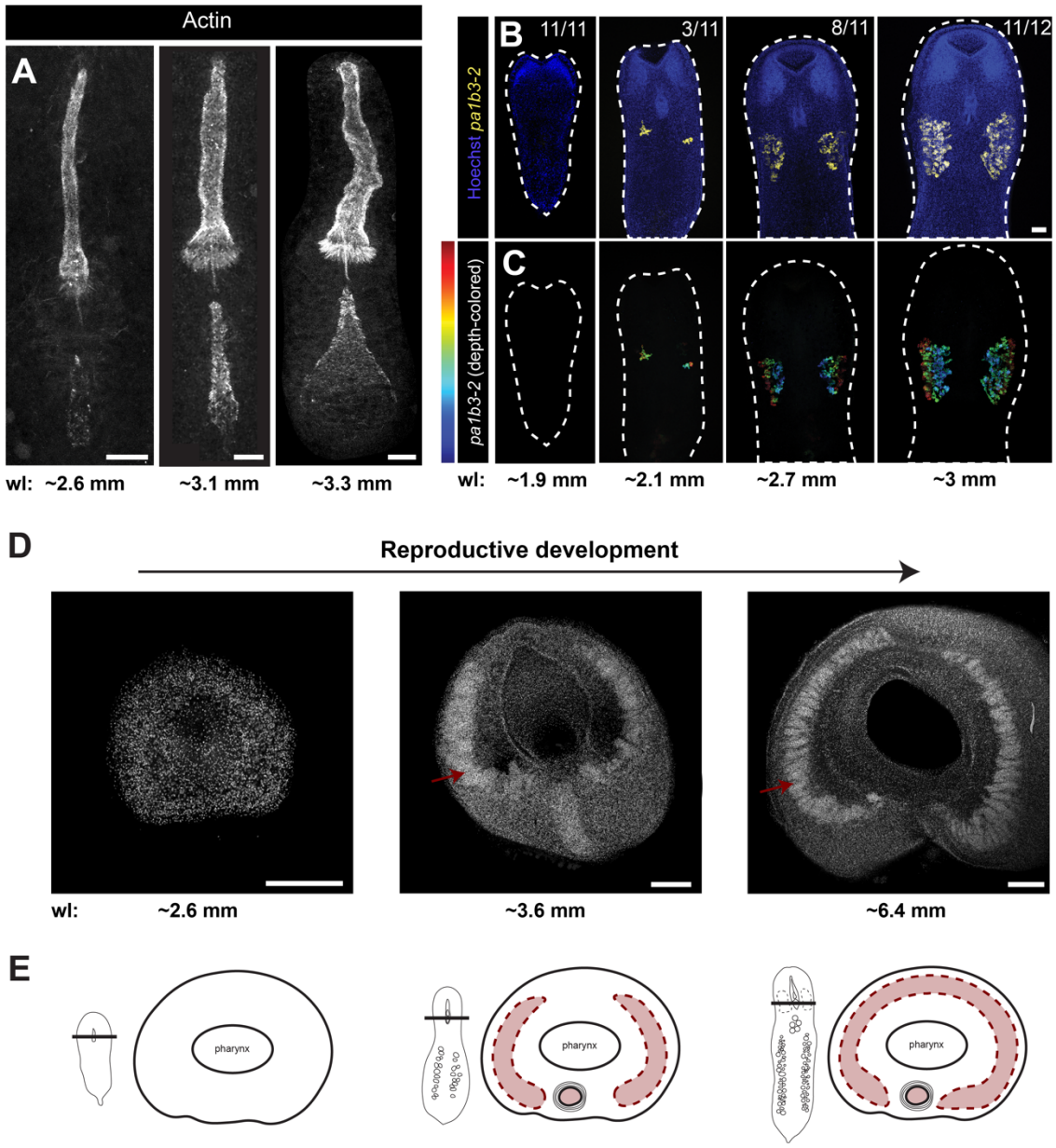

429

430 **Figure 4: Stepwise emergence of individual components of the male reproductive system.** (**A**)
431 Actin-dye labeling shows how the male reproductive system changes over the course of post-embryonic
432 development (shown here from left to right). The sheath and stylets emerge first, followed by the
433 appearance of the prostatic vesicle. (**B**) FISH for the male germline marker *pa1b3-2* results in two regions
434 of ventrolateral expression that extend along the dorsal-ventral axis to different depths. Images are
435 organized by pseudo-time: from least-developed (and smallest) on the left, to most-developed (and
436 largest) on the right. Panels in (**C**) show depth-coloration, showing that the testes extend through the

437 dorso-ventral axis. (**D**) Cross-sections of worms at different points in reproductive development stained
438 with nuclear dye show that testes grow towards the dorsal surface and eventually meet to form one
439 continuous structure. (**E**) Cartoon schematic of cross-sections shown in (**D**). Scale bars: 20μm (A), 100μm
440 (B, C), 200μm (D). Estimated worm lengths (wl) are noted under each panel.
441

442 **Fine structure of the female reproductive system**

443 As observed through imaging of adult worms using a stereo microscope, the female
444 reproductive system in *H. miamia* consists of two lateral ovaries running longitudinally along
445 both sides of the body, and one medial cluster of mature eggs located posterior to the pharynx
446 (Fig. 5A-C). To visualize the structure of the ovaries, we used FISH to label mRNA of a
447 previously-identified germline marker: *cgnl1-2* (Hulett et al., 2023). We found that this gene
448 specifically labeled the oocytes (Fig. 5D). Moreover, immunostaining with a custom antibody
449 against Piwi-1, a stem cell and germline marker, also labeled the ovaries (Fig. 5E). We were
450 also able to visualize the ovaries in histological sections (Fig. 5C). These methods, together with
451 our earlier images of ovaries at different worm ages, showed that oocytes were not organized
452 by maturity within the ovary (Fig. S8A). We did not detect a membrane or lining that envelopes
453 the ovaries. This is consistent with previous work that suggests that acoels lack true ovaries
454 *sensu stricto*: oocytes appear and develop within the parenchymal tissue without a specialized
455 membrane that forms a discrete organ (Eckelbarger and Hodgson, 2021; Rieger et al., 1991;
456 Schmidt-Rhaesa, 2007).

457 Oocytes in *Hofstenia* are surrounded by follicular cells, cells lining developing oocytes
458 that provide nutrition and secrete the eggshell (Bock, 1923; Rieger et al., 1991). We visualized
459 this cell layer with immunofluorescence for Piwi and histology and found that it was consistently
460 present around every oocyte in the ovaries irrespective of their developmental stage (Fig. 5F-G;
461 Fig. S8B-D). We observed that many follicle cells have very large nuclei, perhaps the result of
462 the fusion of neighboring cells (Fig. 5G; Fig. S8B-C). We also found clusters of sperm in the

463 layer of follicular cells surrounding maturing oocytes of a variety of developmental stages (Fig.
464 5F,G, insets), consistent with Bock's (Bock, 1923) proposal that the follicle may 'trap' sperm and
465 control the fertilization of maturing oocytes. We observed significant morphological variation in
466 the cellular components of the oocytes within the ovaries. Early-stage oocytes appeared small,
467 round or oval, although others showed irregular shapes. All oocytes contained a granular
468 substance primarily distributed peripherally and a germinal vesicle occupying a substantial
469 portion of the oocyte (Fig. 5H-J). The presence of a germinal vesicle in the oocytes in *H.*
470 *miamia*'s ovaries suggests that these oocytes are unfertilized. It is likely that oocytes mature in
471 the ovaries, the germinal vesicle breaks down, and then oocytes are fertilized. These mature,
472 fertilized eggs then travel from the ovary to the central cavity prior to being laid.
473 We could not determine conclusively where or when fertilization happens, or where the
474 egg capsule (chorion) is produced. However, the spatial organization of the female reproductive
475 system suggests that an oocyte must mature, become fertilized, and then be transported to the
476 central cavity behind the pharynx. Across our internal examination, we did not identify any
477 oviducts, canals or additional structures that could facilitate this migration from the ovaries to the
478 central cluster. How eggs are transported thus remains unknown.
479

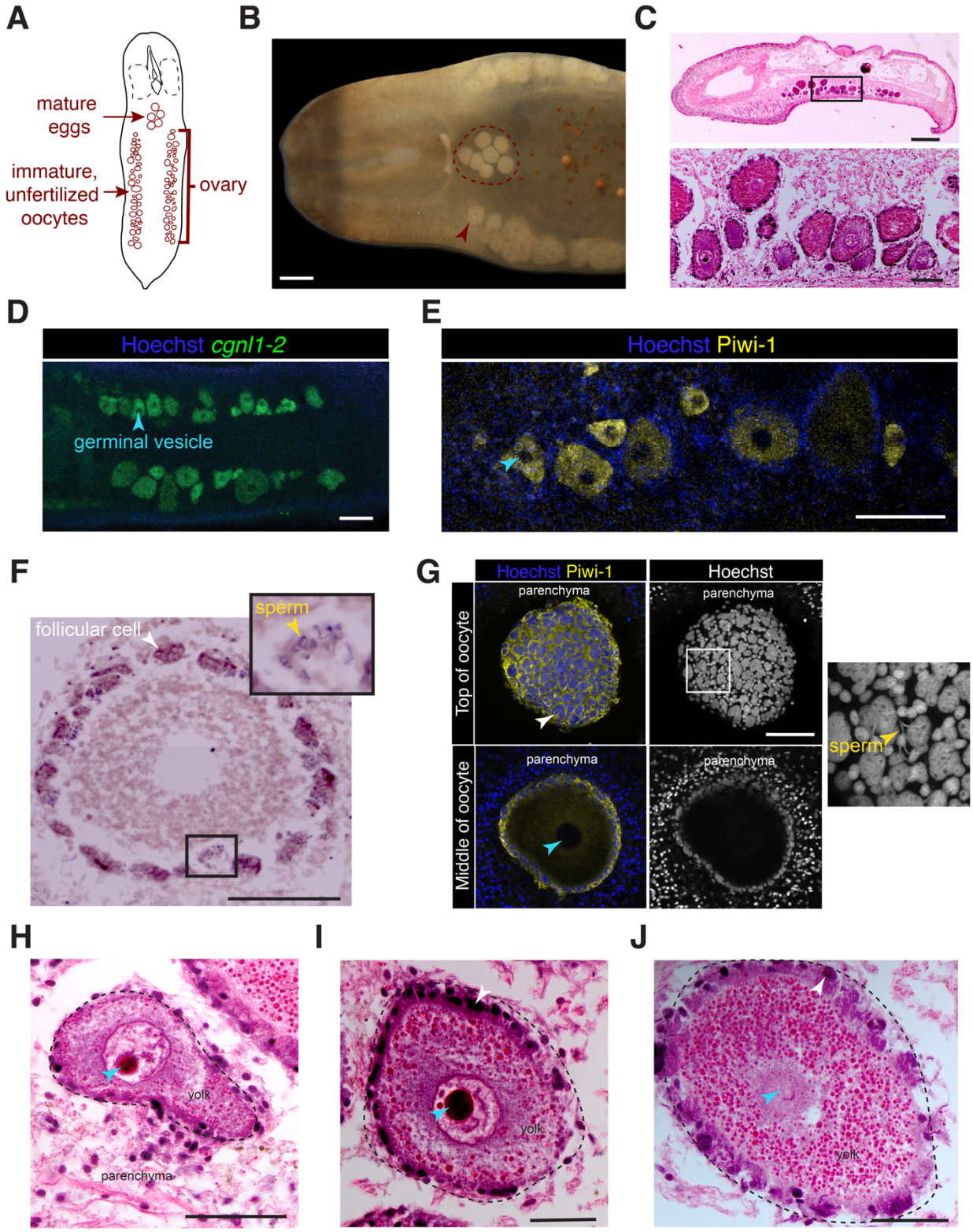

480

481 **Figure 5: The female reproductive system includes embryos stored at the base of the pharynx and**

482 **oocytes in ovaries.** (**A**) A schematized view of the ventral surface of the worm with female reproductive

483 structures highlighted. (**B**) Eggs near the pharynx of the worm (within the red circle) are fertilized and
484 mature while oocytes in ovaries (red arrow) are immature or unfertilized, with a visible germinal vesicle.
485 (**C**) A sagittal histological section shows that the ovaries contain oocytes of varied size and maturity
486 embedded in the parenchyma. (**D**) FISH shows that *cgnl1-2* labels immature oocytes in the ovaries. (**E**)
487 Oocytes in ovaries are also labeled by a Piwi-1 antibody. (**F**) A histological transverse section of an
488 immature oocyte encircled by follicular cells. Inset: sperm cells appear to be trapped in the follicle. (**G**)
489 Piwi-1 immunofluorescence confirms the organization of follicular cells, and nuclear staining sometimes
490 identifies sperm apparently trapped in its surface (inset). Histology also shows that immature oocytes may
491 have irregular shapes (**H**), contain a germinal vesicle (**H,I**), and possess an abundance of (likely yolk)
492 granules (**I,J**). Blue arrows label germinal vesicles in all relevant panels; yellow arrows label sperm; white
493 arrows label follicular cells. Scale bars: 100µm (B, C (inset), D-F), 500µm (C), 50µm (G, H-J)
494

495 **Egg-laying behavior**

496 Egg laying has only been directly observed a few times in acoels, mostly in species within the
497 Convolutidae (Costello and Costello, 1939; Gardiner, 1898). From these observations, acoels
498 are known to lay eggs through the female gonopore (if present) (Gardiner, 1898), a mode of egg
499 laying used by many flatworms (Tong and Ong, 2020), or through breaks in the body wall (Apelt,
500 1969; Costello and Costello, 1939). It has also been suggested that acoels could lay eggs
501 through the mouth; however, direct observation of such egg laying has been challenging (Apelt,
502 1969; Costello and Costello, 1939; Watzin, 1984).

503 Previous authors have speculated that *H. miamia* lay eggs through breaks in the body
504 wall, or perhaps partially through the mouth, but egg laying was not observed (Bock, 1923;
505 Steinböck, 1966). To observe how worms lay eggs, we isolated gravid adult worms and filmed
506 them from underneath for a 24 hour period. 3 worms laid a total of 25 eggs in these conditions.
507 We found that worms exclusively laid eggs through their mouths in events typically lasting less
508 than 2 minutes (Fig. 6A,B; Video 3; Fig. S9A). During this event, the worm performs a series of
509 muscle contractions to transfer a single egg from the ventral pocket of fertilized eggs into the

510 pharynx, and then applies further muscle contractions from posterior to anterior to move the egg
511 to the mouth. The worm then places each egg on the substrate with its mouth, likely secreting
512 mucus to attach the egg to the substrate (Fig. 6A,B; Video 3). Observations from these videos,
513 as well as of egg clutches in our culturing tanks, show that worms can either deposit a single
514 egg in one location or lay eggs in one or more clutches.

515 To understand the temporal dynamics of egg-laying in *H. miamia*, we then quantified the
516 time course of egg-laying in several contexts. We found that adult worms with previous access
517 to mates, once isolated, continued laying eggs for over a month (Fig. 6C). Juvenile worms
518 reared to adulthood in isolation also laid a single burst of eggs (Fig. 6D), multiple months after
519 first being isolated (although the timing of this burst may depend on rearing conditions and the
520 health of the worms). Consistent with our finding that worms reared entirely in isolation can lay
521 eggs (Fig. 1L,M), this burst of egg laying is also likely the result of a selfing event in which the
522 worms fertilize their own eggs, or possibly the result of a form of parthenogenesis allowing the
523 activation of unfertilized eggs. We also allowed virgin worms to mate once, in controlled
524 conditions, and subsequently isolated them. These mated and inseminated worms laid eggs for
525 over three months after a single mating, suggesting that received sperm may be stored in
526 follicular cells for several months (Fig. 6E).

527 Next, we asked how much control the worms had over their egg laying. To test whether
528 worms choose specific locations to lay eggs, we quantified the spatial positions of eggs laid in
529 their culturing tanks. We found that worms have a strong preference for laying eggs on the walls
530 of their containers, rather than on the floor (Fig. 6F). Eggs laid on walls are preferentially laid
531 close to the water line (Fig. 6G, Fig. S9B). This preference is not simply because the worms lay
532 eggs where they are: we observed that worms spend the majority of their time on the floors of
533 their containers, and seem to glide up the walls specifically to lay eggs (Fig. S9C). These spatial
534 preferences do not seem affected by food availability: when deprived of food, egg laying still

535 primarily occurs on the walls of culture boxes (Fig. S9D). These data suggest that worms make
536 active substrate choices for egg laying.
537 We also observed that worms lay 49% of their eggs in clutches. Individual worms can
538 produce these clutches (Video 3). Clutch sizes are often small (Fig. S9E), but the largest can
539 contain over 30 eggs deposited within a 3-4 day window in culture boxes containing 20-50
540 worms (Fig. 6H, Fig. S9E). The vast majority of individual worms lay fewer than 10 eggs in a 3-4
541 day period (Fig. S9F), suggesting that some clutches may be communal. Indeed, in other
542 culturing conditions with large groups of worms, clutch size often exceeds 140 eggs (Fig. 6I). To
543 test whether worms lay eggs in communal clutches, we allowed worms to lay eggs in containers
544 for 3 days. We then swapped worms between containers (or, for control containers, we
545 swapped worms and removed old eggs). We asked how worms interacted with egg clutches laid
546 in the first 3-4 days, and found that many new eggs were laid in pre-existing clutches (Fig. 6J,
547 Fig. S9G). Worms added new eggs to 42 percent of old egg clutches. This shows that worms
548 frequently lay eggs in communal egg clutches.
549 Finally, we asked whether worms withhold eggs in suboptimal environments. Our
550 observations (see Fig. 2K-L) suggested that worms are physiologically resilient to food stress.
551 We therefore conducted an experiment with a set of worms, half of which were deprived of food
552 for one feeding period (3-4 days). The other set was fed normally during this period. We found
553 that food-deprived worms laid significantly fewer eggs during this period (Fig. 6K). We
554 hypothesized that this reduction in egg-laying was because the worms were actively withholding
555 their eggs in the absence of food. Next, we repeated this experiment, first depriving some
556 worms of food and subsequently feeding them. After food-deprived worms were given food, they
557 laid an excess of eggs (Fig. 6L), showing that the worms withhold egg-laying in food-limited
558 environments. More generally, these data show that *H. miamia* assess their environments to
559 decide when and where to lay eggs.
560

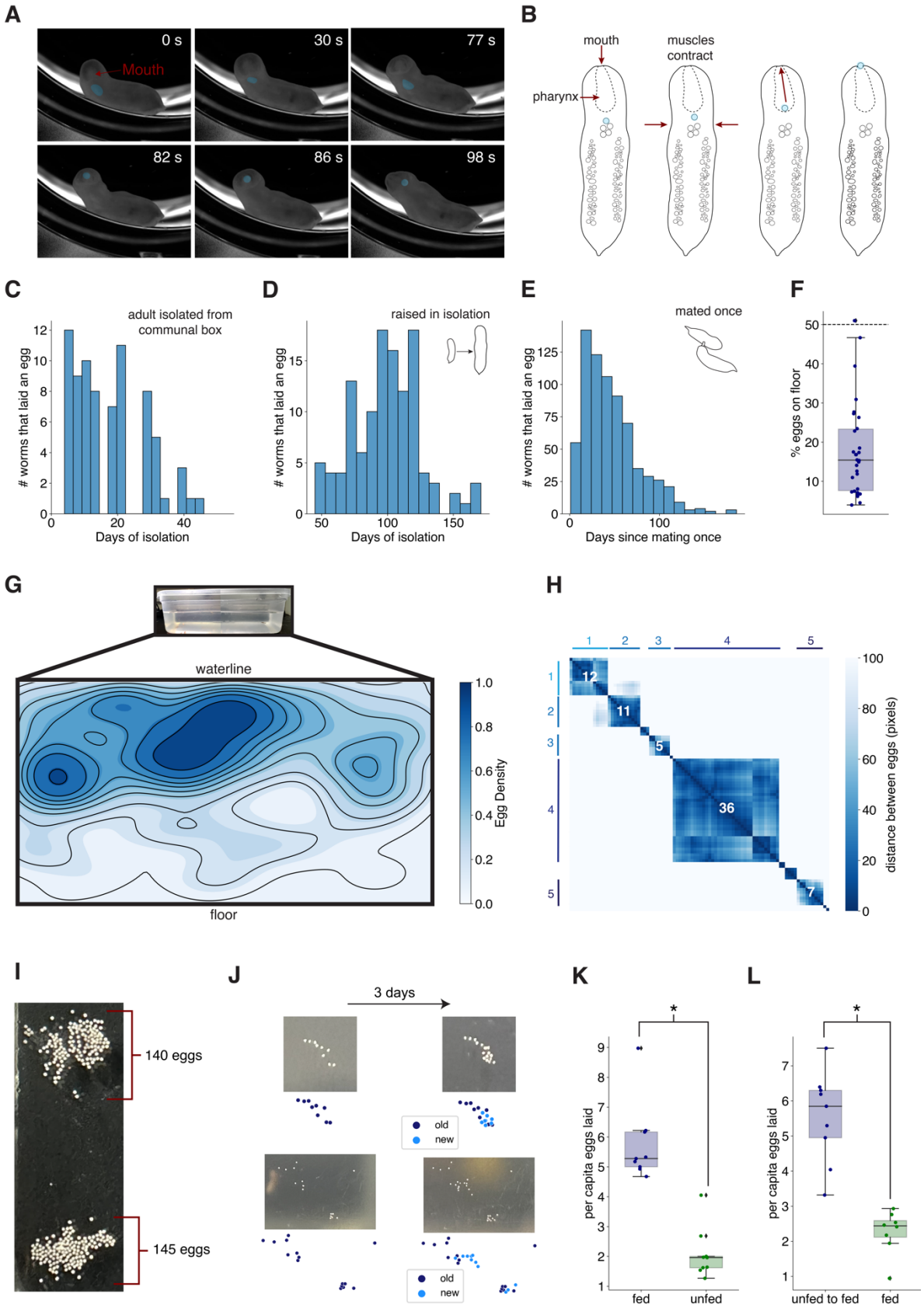
A
0 s
30 s
77 s
Mouth
82 s
86 s
98 s
B
mouth
muscles contract
pharynx
C
adult isolated from communal box
worms that laid an egg
Days of isolation
D
raised in isolation
worms that laid an egg
Days of isolation
E
mated once
worms that laid an egg
Days since mating once
F
% eggs on floor
G
waterline
floor
Egg Density
H
distance between eggs (pixels)
I
140 eggs
145 eggs
J
3 days
old
new
old
new
K
per capita eggs laid
fed
unfed
L
per capita eggs laid
unfed to fed
fed

562 **Figure 6: *H. miamia* lays eggs through the mouth and exhibits environmental preferences in egg**
563 **laying.** (**A**) Sequence of images from a video of egg-laying through the mouth. Eggs in the pharynx and
564 emerging through the mouth are shaded blue. (**B**) Schematic showing presumed process of embryo
565 traveling from the cavity beneath the pharynx to the pharynx and then out through the mouth. (**C**)
566 Histogram showing the timing of eggs laid by adult worms living in communal tanks and then isolated. (**D**)
567 Histogram showing the timing of eggs laid by worms that undergo reproductive development in isolation
568 and then self-fertilize. (**E**) Histogram showing the timing of eggs laid by worms that are allowed to mate
569 once. (**F**) Scatterplot of the percentage of eggs found on the floor of communal tanks ($n = 30$). This is
570 significantly different from the expected percentage of eggs based on tank surface area (t-test $p <$
571 0.0001). (**G**) Kernel density estimate of egg locations on a subset of tank surfaces with similar dimensions
572 ($n = 2144$ eggs). (**H**) Density-based spatial clustering of egg coordinates shows that eggs are laid in
573 clutches. Number of eggs in a clutch shown in white. (**I**) In some culturing conditions, worms lay clutches
574 of up to 145 eggs. (**J**) New worms add eggs to pre-existing clutches laid by other worms. (**K**) Worms that
575 are unfed for 4 days lay fewer eggs than fed worms ($n = 9$ tanks, t-test $p < 0.0001$). (**L**) Unfed worms that
576 are subsequently fed lay more eggs than worms that are continuously fed ($n \geq 8$ tanks, t-test $p < 0.0001$).

Discussion

Our work describes the reproductive life history of an acoel across its life cycle (Fig. 7A). We reveal many new facets of acoel biology, describe the structure and dynamics of growth, regeneration, and egg-laying behavior, and establish a foundation for the experimental study of reproductive biology in acoels. Below, we discuss the significance of our findings for reproductive development, behavior, and the evolution of life history strategies.

Reproductive development and regeneration

Little is known about the development or regeneration of reproductive structures in acoels. Our data show that in *H. miamia*, reproductive structures develop and regenerate in a stereotyped sequence, with male organs appearing before female ones. During starvation-induced de-growth, these organs degenerate in the opposite sequence. This stereotypy is unexpected and may not be a universal feature of acoels: sparse data from three other acoel species, *Solenofilomorpha funilis* (Crezée, 1975), *Otocelis luteola* (Kozloff, 2000a) and *Aphanostoma pulchra* (Perea-Atienza et al., 2013), indicate that these species do not exhibit identical sequences. The stereotypy we observe is consistent with the idea that a single, size-associated program regulates reproductive organ development in *H. miamia*, and that it may be deployed in a variety of growth contexts.

Our results also show that *H. miamia* is capable of regenerating all reproductive structures from a variety of initial tissue configurations. The trajectories toward organ replacement vary based on this initial state, and reveal important features of the regenerative process. For instance, we found that worms missing their sagittal halves or their tails first shrink in size before re-growing. This may be in part because the early stages of wound closure and regeneration require the reorganization of existing tissues. In any case, this reduction in body size is associated with disproportionate reductions in reproductive organ size, demonstrating active tissue destruction

603 mechanisms, possibly mediated by apoptotic processes similar to those reported in other
604 regenerative species (Ballarin et al., 2008; Pellettieri et al., 2010; Rychel and Swalla, 2008). In
605 addition, we found that the two ovaries within a worm grow in a significantly correlated manner,
606 and after sagittal amputation, the missing ovary grows disproportionately to regenerate
607 symmetry. In principle, such bilateral symmetry could be achieved passively, without any
608 feedback (Reddien, 2018). However, the strong within-worm correlation, even after controlling
609 for body size, suggests that there is either organism-specific coordination of growth or death
610 rates, or more likely a feedback process that ensures bilateral symmetry.
611
612 In many animal lineages such as arthropods, vertebrates, planarians, and nematodes, organs
613 typically grow symmetrically, and scale with body size (Boulan and Léopold, 2021; Ko et al.,
614 2024; Uppaluri and Brangwynne, 2015; Wolpert, 2010). The mechanisms underlying this
615 coordinated, scaled growth are not fully understood, and may vary across tissues and species.
616 For instance, some vertebrate tissues appear to grow using cell-intrinsic programs; others - and
617 many insect tissues - appear to rely on central coordinating mechanisms that read signals of
618 growth from the circulation or from unknown sources (Allard and Tabin, 2009; Boulan and
619 Léopold, 2021; Harris et al., 2021; Trible and Kronauer, 2017; Vallejo et al., 2015; Wolpert,
620 2010). How different organs ensure appropriate, coordinated scaling remains poorly
621 understood. We find that *H. miamia* must also solve this problem: their reproductive organs
622 scale with body size during development, regeneration, and de-growth, and an active
623 coordination mechanism ensures that the ovaries return to symmetry after perturbations. How
624 do tissues across the body 'read' the same indicators of size, and how is their growth
625 coordinated? Our work establishes a foundation for the experimental study of these and other
626 developmental phenomena.
627
628 **Egg-laying physiology and behavior**

629 Despite speculation, few acoels have been directly observed laying eggs (Costello and Costello,
630 1939; Gardiner, 1895; Watzin, 1984). We find that *H. miamia* lays fertilized eggs through its
631 mouth: a mode of egg-laying not found in other animals. This unusual behavior raises multiple
632 questions. First, where in the animal does fertilization occur? Our observations suggest that
633 follicular cells surrounding immature oocytes may act as a selective barrier to sperm, preventing
634 many sperm cells from reaching the oocyte, a function suggested by Bock (1923). Additionally,
635 given that *H. miamia* can lay eggs for months after a single mating despite lacking a seminal
636 bursa, it is likely that the follicular cells function as a sperm storage organ. Second, we find that
637 *H. miamia* appears capable of self-fertilization, as it can lay eggs without mating. While some
638 acoels are capable of asexual reproduction through fissioning and budding (Åkesson et al.,
639 2001; Ax and Schulz, 1959; du Bois-Reymond Marcus, 1955; Hanson, 1960; Ishikawa and
640 Yamasu, 1992; Zabotin and Evtugyn, 2021), self-fertilization has not been reported previously.
641 How does sperm travel to the ovaries? It is likely that sperm cells migrate posteriorly from the
642 testes towards the ovaries in isolated worms, and from arbitrary body regions towards the
643 ovaries after mating. In addition, sperm must travel from all regions of the testes to the seminal
644 and prostatic vesicles. Whether they use chemical cues to navigate towards oocytes and these
645 vesicles, and the mechanics of this process, remain unknown. Third, how do mature eggs travel
646 from the lateral ovaries to the central cavity, and how are the eggs in this cavity physically
647 loaded into the pharynx? Our anatomical observations have so far failed to reveal obvious
648 oviducts, or other tube-like structures that could facilitate movement of eggs into the pharynx.
649 The only known opening at the posterior of the pharynx is the pharyngeal sphincter that allows
650 food to pass into the gut. We therefore speculate that eggs travel through the gut to the central
651 cavity, which may simply be a pocket within the gut. Eggs may then be moved into the pharynx
652 through a form of reverse peristalsis (and observation of the worm prior to egg-laying shows
653 waves of muscle contraction proceeding posterior-to-anterior as each egg is loaded into the
654 pharynx).

We also find that *H. miamia* appears to make active choices about when and where to lay fertilized eggs. *H. miamia* has clear spatial preferences for egg-laying in our culture chambers. Worms often lay eggs in communal clutches, sometimes adding to another worm's clutch. They also have environmental preferences, withholding egg-laying when deprived of food and then quickly laying eggs once food is present again. Together, these results show that *H. miamia* surveys its environment and then integrates this assessment into whether - and where - it is suitable to lay an egg. More generally, the existence of communal egg clutches raises the possibility that acoels may have a rich and unexplored social repertoire.

Evolution of reproductive strategies within acoels

Placed in a comparative context, our description of *H. miamia*'s reproductive life history reveals that acoels and their sister lineage, the nemertodermatids, display a striking diversity of reproductive morphologies, and likely a corresponding diversity in reproductive behavior (Fig. 7B). This diversity reveals correlated suites of reproductive traits that suggest a small number of life history strategies. For instance, the presence of a bursa and female gonopore are associated with a muscular penis, suggestive of cooperative, genital-handshake style mating. The absence of a bursa and female gonopore are associated with a needle-laden penis, suggestive of competitive, hypodermic-insemination style mating. Comparative work in the distantly-related flatworms shows that these anatomical and behavioral traits indeed coevolve similarly (Brand et al., 2022a, 2022b), in accordance with social evolutionary theory on sexual conflict (Charnov, 1979; Michiels and Newman, 1998; Ramm et al., 2015). Within the genus *Macrostomum*, a competitive hypodermic insemination syndrome has evolved at least 14 times from ancestral cooperative, reciprocal insemination (Brand et al., 2022a, 2022b). This syndrome involves the correlated evolution of a sharpened penis, a simplified female sperm-receiving organ, sperm cells lacking bristles and other adaptations for post-copulatory sexual conflict, and

associated behavioral changes (Brand et al., 2022a, 2022b, 2022c; Schärer et al., 2014, 2011). Whether similar anatomical associations truly predict mating strategies in acoels remains unknown. In addition, the variability of some morphological features does not obviously fit this pattern of cooperative vs competitive reproductive strategies. For example, the relative locations of the testes and ovaries is highly variable, as is the number of bursal nozzles, suggesting that there may be further evolutionary patterns awaiting explanation. Our work establishes an approach to study reproductive anatomy and behavior in a model acoel. This approach can be applied to many other acoel species. Given their rich diversity, acoels are a promising clade in which to study the evolution of reproductive strategies, and in which to test the generality of theories of sexual conflict.

Conclusion

These findings establish foundational knowledge of anatomical, physiological, and behavioral elements of *H. miamia*'s reproductive life history. This enables future work on the molecular genetics of reproductive organ development and regeneration, on the physiological processes involved in egg maturation and oviposition, and on the neuroscience of reproductive behavior.

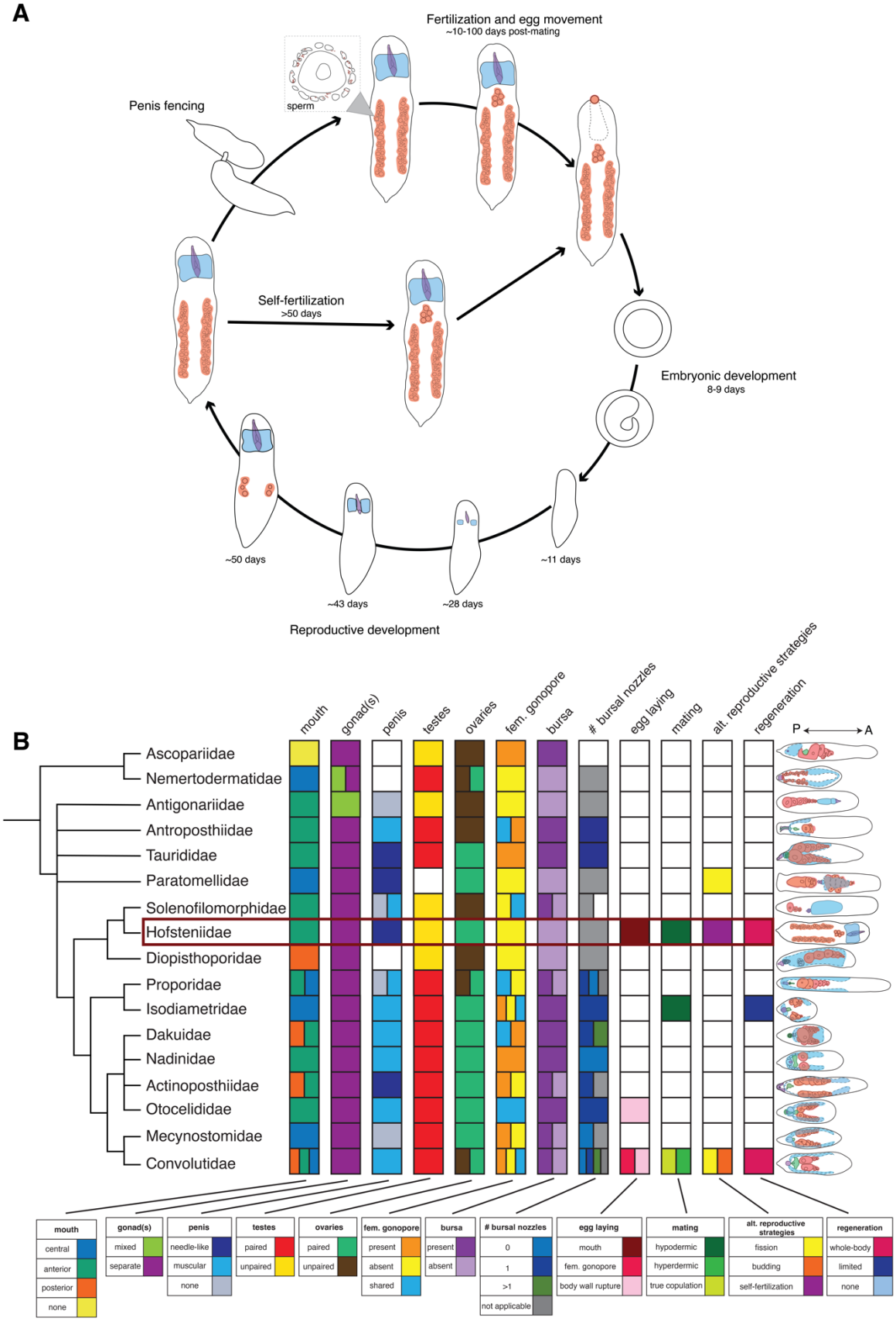
A
Fertilization and egg movement
~10-100 days post-mating
sperm
Penis fencing
Self-fertilization
>50 days
Embryonic development
8-9 days
~50 days
~43 days
~28 days
~11 days
Reproductive development
B
mouth
gonad(s)
penis
testes
ovaries
fem. gonopore
bursa
bursal nozzles
egg laying
mating
alt. reproductive strategies
regeneration
P
A
Ascopariidae
Nemertodermatidae
Antigonariidae
Antroposthiidae
Tauididae
Paratomellidae
Solenofilomorphidae
Hofsteniidae
Diopisthoporidae
Proporidae
Isodiametridae
Dakuidae
Nadinidae
Actinoposthiidae
Otocelididae
Mecynostomidae
Convolutidae
mouth
central
anterior
posterior
none
gonad(s)
mixed
separate
penis
needle-like
muscular
none
testes
paired
unpaired
ovaries
paired
unpaired
fem. gonopore
present
absent
shared
bursa
present
absent
bursal nozzles
0
1
>1
not applicable
egg laying
mouth
fem. gonopore
body wall rupture
mating
hypodermic
hyperdermic
true copulation
alt. reproductive strategies
fission
budding
self-fertilization
regeneration
whole-body
limited
none

Figure 7: Reproductive life histories in Acoelomorpha. (A) The life cycle of *Hofstenia miamia*, with major reproductive events displayed. **(B)** Family-level phylogeny of Acoelomorpha (Nemertodermatida, Acoela) showing anatomical and reproductive life history traits (Table S1): position of the mouth, whether gonads are mixed or separated by sex, penis type, paired or unpaired testes, paired or unpaired ovaries, presence or absence of a female gonopore, presence or absence of a seminal bursa, the number of associated bursal nozzles, egg-laying mode, mode of sexual reproduction, alternative reproductive strategies, and regenerative capacity (see Table S4 for definitions of terms and categories). Schematic diagram of the reproductive anatomy of representative species from each family within Acoelomorpha with specific structures colored: male copulatory organ (purple), sperm in testes and/or seminal vesicle (blue), oocytes (red), female or shared gonopore and/or bursa (green). (Table S1). White boxes represent unknown phenotypic states, and in the case of asexual reproduction, its possible absence. Phenotypic classifications are from (Achatz and Hooge, 2006; Apelt, 1969; Bailly et al., 2014; Beltagi and Mandura, 1991; Bock, 1923; Boone et al., 2011; Bush, 1975; Costello and Costello, 1939, 1938; Crezee, 1978; Dörjes, 1968, 1966; Faubel, 1976, 1974; Faubel and Cameron, 2001; Gardiner, 1895; Grae and Kozloff, 1999; Hooge, 2003; Hooge et al., 2007; Hooge and Smith, 2004; Hyman, 1937; Kostenko, 1989; Kozloff, 2000b; Meyer-Wachsmuth et al., 2014; Peebles, 1915; Perea-Atienza et al., 2013; Raikova et al., 1995; Riser, 1987; Shannon and Achatz, 2007; Steinböck, 1966; Sterrer, 1998; Watzin, 1984)**.**

Methods

Animal husbandry

We reared gravid *H. miamia* in communal plastic 2.25 L boxes with approximately 1.25 L of artificial seawater (37 ppt, pH 7.8-8.2). These communal tanks were kept in incubators held at 21°C. Twice weekly, we collected embryos, changed their seawater, and fed them with *Artemia* sp. (brine shrimp). The embryos were raised in petri dishes. Once they hatched, we transferred

726 juvenile worms to tanks maintained at room temperature and fed them with marine rotifers
727 (*Brachionus plicatilis*). When reproductive organs began to develop, we transferred worms to
728 larger tanks, each typically housing 30-50 worms. To pair animals for mating, we transferred
729 juvenile worms from tanks to 24-well plates and reared them in isolation following similar
730 feeding and cleaning routines as listed above. In order to study the regeneration of reproductive
731 systems, we isolated adult worms from communal tanks, anesthetized them in 15% tricaine
732 (ethyl 3-aminobenzoate methanesulfonic acid), and then amputated them with micro knives
733 (Fine Science Tools #10316-14). We maintained regenerating worm fragments in 6-well plates
734 and cleaned plates twice weekly. Five days after amputation, we fed these worms *Artemia* sp.
735 (brine shrimp) or rotifers. We also maintained starving animals in 6-well plates that we cleaned
736 twice weekly but that were not fed. All animals are derived from an inbreeding population of
737 worms collected in 2010 from Bermuda.
738
739 **Histology**
740 We fixed adult specimens of *H. miamia* in 4% paraformaldehyde in artificial seawater for 24
741 hours at room temperature. Following fixation, specimens were washed twice with 70% ethanol
742 to remove the fixative and then preserved in a third change of 70% ethanol for histological
743 preparation. Animals were dehydrated through a graded ethanol series (95% and 100%),
744 cleared in Histoclear, and embedded in Leica Surgipath (Paraplast) with a melting point of 56°C.
745 We made longitudinal, transverse, and sagittal sections at a thickness of 5 µm using a Leitz
746 1512 microtome. We stained these sections using a standard protocol with hematoxylin and
747 eosin, mounted them on glass slides with Permount, and imaged them using a Zeiss Axio
748 Scan.Z1, and an Olympus BX50 microscope.
749
750 **Fluorescence *in situ* hybridization (FISH)**

751 We synthesized riboprobes following protocols established in (Srivastava et al., 2014).
752 Following 1-2 weeks of starvation, we fixed whole worms in 4% paraformaldehyde in artificial
753 sea water for one hour at room temperature. We then washed the fixed animals with PBST
754 (PBS + 0.1% Triton-X-100) and transferred them to 24-well plates in small baskets with a mesh
755 bottom, with 4-6 animals in each basket. To remove pigment autofluorescence, we treated the
756 animals with a bleach solution (containing 4% hydrogen peroxide, SSC, and formamide) and left
757 them under a light for two hours. For all washes, 800 µL of solution was used. We first
758 permeabilized the animals using proteinase K solution (0.1% SDS, 1 µL/10 mL proK in PBSTx).
759 After 10 minutes, we post-fixed the worms in 4% formaldehyde in PBST, washed twice in PBST,
760 and then washed in a 1:1 PBST:PreHyb solution for 10 minutes. We then incubated the
761 samples in PreHyb solution (50% DI formamide, 25% 20X SSC, 0.05% 10% Tween-20, 1mg/mL
762 yeast tRNA, 20% water) for two hours in a 56°C hybridization oven and then transferred them to
763 a hybridization solution (50% DI formamide, 25% 20X SSC, 0.05% 10% Tween-20, 1 mg/mL
764 yeast tRNA, 10% 50% dextran sulfate, 10% water) containing riboprobe(s) overnight. We then
765 put the specimens through several 30-minute washes at 56°C, starting with two PreHyb
766 washes, two 1:1 PreHyb:2XSSCT washes, two 2XSSCT (2XSSC with 0.1% TritonX-100)
767 solution washes, two 0.2XSSCT (0.2X SSC with 0.1% TritonX-100) solution washes. We cooled
768 the specimens to room temperature and then washed them in two ten-minute PBST washes.
769 We then performed a 1-hour blocking at room temperature with blocking solution (5% horse
770 serum and 5% casein in PBST). We incubated specimens with anti-Digoxigenin-POD (1:1500
771 dilution; Roche, 11633716001) in a blocking buffer overnight. The following day, we washed
772 animals 6 times with PBST, incubated with a tyramide buffer (1.1688g/mL NaCl, 6.18mg/mL
773 boric acid, filled with water and adjusted pH to 8.5) for 10 minutes, then developed with
774 rhodamine-conjugated tyramide solution for 10 minutes. We washed animals again with PBST
775 and incubated for 1 hour in 1:500 PBST:Hoechst to label nuclei. We mounted the animals on
776 glass slides with VECTASHIELD® PLUS Antifade Mounting Medium (Vector Laboratories, H-

777 1900). We estimated worm length (Fig. 4A-D) by measuring copulatory apparatus length
778 (gonopore to prostatic vesicle) or cross-sectional worm width within the image and comparing
779 that measurement to measurements of developing worms.
780
781 **Whole-mount immunofluorescence**
782 We fixed worms in 4% paraformaldehyde (Electron Microscopy Sciences, 15714) in artificial sea
783 water for 1-2 hours at room temperature (juveniles were fixed for one hour, adults were fixed for
784 two) before washing with PBST (PBS + 0.1% Triton-X-100). We anesthetized adult worms in 0.5
785 mg/mL tricaine for 5 minutes prior to fixation to minimize epidermal rupture. For
786 immunofluorescence, we washed worms in PBST, blocked for one hour at room temperature in
787 10% goat serum in PBST, and incubated them in primary antibody for 48-72 hours at 4°C on a
788 shaker (juveniles for 48 hours, adults for 72 hours). The following day, we washed worms
789 thoroughly in PBST (8 x 20 min washes) on a nutator before blocking for one hour at room
790 temperature on a shaker. We incubated worms in secondary antibody overnight at 4°C; the
791 following day, we washed them thoroughly in PBST (8 x 20 in washes) on a shaker before
792 adding direct conjugate dyes and mounting them on glass slides with VECTASHIELD®
793 HardSet™ Antifade Mounting Medium (Vector Laboratories, H-1400-10). We used the following
794 antibodies: Tropomyosin (custom) (Hulett et al., 2020), Piwi-1 (custom), Goat anti-Rabbit IgG
795 (H+L) Cross-Adsorbed Secondary Antibody, Alexa Fluor™ 568 (ThermoFisher, A-11011),
796 Hoechst (ThermoFisher, H1399), SiR-actin (Cytoskeleton, CY-SC001). We acquired all images
797 with FISH and immunofluorescence on a Leica SP8 point-scanning confocal microscope. We
798 generated the Piwi-1 (Rabbit polyclonal) custom antibody using GenScript as previously
799 described for Tropomyosin (Hulett et al., 2020). Briefly, a peptide was synthesized from the *H.*
800 *miamia* Piwi-1 protein sequence, expressed in *E. coli,* and used to immunize rabbits. The Piwi-1
801 antibody used in this paper was #SC1195 (0.845 mg/mL), used at the concentration of 2 ug/mL.
802

803

804 **Quantitative analysis of development, regeneration, and de-growth**

805 We collected 42 zygotes laid from wild-type worms. Two embryos did not hatch, and two worms
806 died during the course of the experiment (likely due to handling error). Four worms were
807 removed from the experiment at different timepoints for additional imaging, resulting in 34
808 worms that we followed into adulthood (Fig. S2B). We transferred each embryo to a well of a
809 24-well cell culture plate with artificial seawater. Plates were stored in a temperature-controlled
810 incubator. Without removing the embryos from the plate, we imaged them twice weekly through
811 a dissection microscope with white illumination from LEDs mounted above the sample. We also
812 changed water on these days. We added the same volume of water to each well (2.35 mL in
813 each 12-well). Once at least one embryo had hatched, we added rotifers to each well. On each
814 feeding day, we calculated the concentration of rotifers by counting the number of rotifers in
815 diluted samples. Based on this concentration, we changed the volume of rotifers added to each
816 well to ensure a consistent number of rotifers was given to each animal. At different stages
817 during the experiment, we increased the number of rotifers (Fig. S2A). These increases were
818 gradual to ensure worms always had more food than they could eat, while minimizing excess
819 food which could affect water quality. We removed hatched worms from wells for imaging twice
820 weekly. We anesthetized worms in tricaine, and mounted them on microscope slides with a
821 20x20 mm sticker grid with 1mm resolution (ThomasScientific, #1207X53). Depending on the
822 worms' pigmentation, this grid is visible through the body of some worms, but this did not impact
823 the visibility of reproductive organs. When worms were larger, we moved them to larger 6-well
824 plates in 10 mL of artificial sea water and began to feed them brine shrimp in addition to rotifers
825 (Fig. S2A). We measured the number of brine shrimp added using the same concentration
826 procedure outlined above for rotifers. Once worms had matured, we increased the number of
827 brine shrimp.

We manually annotated images in FIJI. We measured lengths from the most posterior part of the male reproductive system (e.g., base of the penis tube before sperm production begins or base of the seminal vesicle) to the male gonopore, the length of the seminal vesicle, the length of each ovary, the length of the worm's body, and the width of the worm's body. We calculated penis length by subtracting the length of the seminal vesicle from the length of the male gonad. All measurements were converted to millimeters using image-specific scale information.

We repeated these imaging and measurement processing procedures with starving worms and regenerating worm fragments. We anesthetized and imaged starved and fed control worms roughly once a week for 11 weeks. 106 days after isolation, we imaged the starved worms again, at which point one starved worm had died. We imaged regenerating worms starting 2 days post-amputation and then again every 2-5 days until 25 days post-amputation at which point we took images less frequently. We did not feed regenerating fragments for the first four days after amputation, and then fed them normally. In these experiments, we used a two-pointed line or multi-jointed spline to measure lengths. We performed all analyses in python, with code assistance from GPT4.

Egg-laying behavior

We moved adult worms from a communal tank to individual wells in the center of a 24-well plate or 12-well plate (Fisher Scientific #07-200-82). We mounted the plate on an elevated platform within an enclosed behavioral rig. The plate was illuminated with uniform white light, from addressable LEDs (Adafruit #SK6812RGBW, powered by 5V DC) arranged in a ring around the plate behind a white acrylic diffuser (McMaster-Carr #8505K741). An infrared camera (Basler Ace ac4024-29um USB 3.0 monochrome) was mounted underneath the plate to allow filming of the worm's ventral surface. A USB fan was mounted on the floor of the behavioral chamber for

853 temperature regulation. We filmed worms at 1Hz for 8-12 hours. After filming, each worm was
854 returned to its original communal tank.

855 To determine the timing of egg laying in adults with continuous access to mates, we
856 collected adult worms from communal tanks and each was placed in an individual well of a 6-
857 well plate. Every 3-4 days, we counted the number of eggs laid by each worm, removed the
858 eggs, changed the water, and fed worms with brine shrimp or rotifers. To induce self-
859 fertilization, we moved juvenile worms with immature reproductive systems from communal
860 tanks to 24-well plates and fed them with rotifers. Once these worms had increased in size, we
861 moved them to 6-well plates and fed with artemia. We recorded egg counts every 3-4 days
862 when water and food were refreshed. To determine the time course of egg laying after mating
863 once, we isolated juvenile worms. Once these worms were reproductively mature, we paired
864 each worm with another isolated worm and allowed them to mate. After mating, we returned the
865 worms to isolation. We recorded egg counts as previously described. If worms stopped laying
866 eggs for more than two weeks, we allowed them to mate again before re-isolating them.

867 To find egg positions, we maintained communal tanks according to our husbandry
868 protocol. Every 3-4 days, before cleaning, we recorded images of each face of the tank (2 short
869 faces, 2 long faces, and the floor of the tank). We then scored the x- and y-coordinates of eggs
870 on each face using FIJI. Since few eggs were laid on the floors of the tanks and it was unclear
871 whether these eggs were attached or had been dislodged from the walls of the tanks, we did not
872 score their locations (Fig. 6F). We also scored the x- and y-coordinates of the boundaries of the
873 water in each image. From these image-specific boundaries, we calculated a common set of
874 bounds for each type of face (i.e., short, long). We scaled egg coordinate positions and aligned
875 them to common bounds for analysis of spatial egg laying preferences. To ask whether worms
876 add to existing clutches of eggs, we cared for communal tanks as previously described but did
877 not remove eggs from their faces. We took images of each face, and then we transferred each

878 cohort of worms in a tank to a different tank. After 3-4 days, we took images of tank faces again,
879 scored coordinates of each egg, and recorded whether each egg was old or newly laid.
880 For experiments measuring how worms altered their egg-laying behavior based on food
881 availability, we selected 17 and 18 communal worm tanks respectively. On the first day of the
882 experiment, half of these tanks were randomly selected to have food (brine shrimp) withheld.
883 After four days with or without food, we collected and counted eggs from all boxes. To test
884 whether egg laying recovers when unfed worms are fed, we randomly selected communal tanks
885 of adult worms to have food withheld. Four days after food was added or withheld, we removed
886 all eggs that were laid, and then fed all communal tanks. Three days later, eggs were collected
887 and counted.
888
889
890 **Author Contributions**
891 VC, SET, and MS designed the project; SET and VC performed development, physiology and
892 behavior experiments; VC and SET analyzed the data; APK performed and interpreted
893 immunofluorescence and imaging experiments; DMB performed and interpreted histology
894 experiments; VC, SET, and MS wrote the manuscript with input from all authors; and MS
895 supervised the project.
896
897 **Acknowledgements**
898 We thank Gonzalo Giribet, Matthew Hooge, James Hanken, Javier Ortega-Hernandez, Andrew
899 Berry, and all members of the Srivastava lab for helpful discussion. We also thank James
900 Hanken, Júlia Chaumel, and Christina Daly for histology help and infrastructure. VC and APK
901 are Fellows of the Jane Coffin Childs Fund for Medical Research. ST acknowledges funding
902 from the Harvard Museum of Comparative Zoology, Herchel Smith Undergraduate Science
903 Research Program, and the Program for Research in Science and Engineering. This project

904 was supported by grants from the National Institute of General Medical Sciences of the NIH to
905 MS: R35GM128817 and R35GM153252.

906

907

908 ## Supplement

909 **Table S1: Survey of reproductive traits within Acoelomorpha.** see attached .xlsx file

910

911 **Table S2: Body length is a better predictor of organ length than age in multiple**
912 **regression.** Multiple regression coefficients and associated p-values are reported for each
913 organ. Wald's test was used on coefficients to test whether they are significantly different from
914 each other.

organ	day coefficient	day p-value	worm length coefficient	worm length p-value	wald's test p-value
penis	0.0684	0.0002	0.1639	<0.0005	0.0082
seminal vesicle	0.0425	0.0003	0.0985	<0.0005	0.0128
ovary	0.3361	<0.0005	1.0029	<0.0005	<0.0005

915
916

917 **Table S3: ANCOVA of the relationship between organ size and body size.**

	F-statistic	p-value	η^2
penis	15.82	<0.0005	0.040
seminal vesicle	24.329	<0.0005	0.069
ovary	58.905	<0.0005	0.175

918

919 **Table S4: Glossary of anatomical and reproductive traits.**

mouth: approximate position of the mouth on the ventral surface

central	mouth located between the anterior end and midpoint of the ventral surface
anterior	mouth located between the anterior end and midpoint of the ventral surface
posterior	mouth located between the midpoint of the ventral surface and posterior end
none	no mouth
gonad(s): tissue or organ where gametes are specified	
mixed	sperm and eggs are produced within the same tissue or organ
separate	sperm and eggs are produced in distinct tissues or organs
penis: male copulatory organ	
needle-like	penis contains hardened, sclerotized elements
muscular	absence of hardened elements; soft or glandular penis
none	penis is absent
testes: tissue where sperm are produced	
paired	there are two distinct regions where sperm are produced
unpaired	there is a single region where sperm are produced
ovaries: tissue where oocytes are produced	
paired	there is are two distinct regions where oocytes are produced
unpaired	there is a single region where oocytes are produced
fem. gonopore: female genital opening	

present	a female genital opening is present
absent	a female genital opening is not present
bursa: an organ used to hold sperm received during mating	
present	a bursa is present
absent	a bursa is not present
# bursal nozzles: the number of channels accompanying the bursa; channels that facilitate sperm movement or modification	
0	the bursa is not accompanied by any sperm channels
1	the bursa has one channel used to move sperm
>1	the bursa has more than one channel used to move sperm
egg laying: the mode of oviposition that a species has been observed to use	
mouth	eggs are deposited via the mouth
fem. gonopore	eggs are deposited via the female genital opening
body wall rupture	eggs are deposited via breaks in the body wall
mating: the mode of sexual reproduction that a species has been observed to use	
hypodermic	a copulation mode where sperm is injected beneath the epidermis of a partner
hyperdermal	a copulation mode where sperm are deposited on the epidermis of a partner
true copulation	penis inserted in the female gonopore of a partner; insertion can be mutual or one-sided

alt. reproductive strategies: forms of reproduction other than two individuals mating	
fission	splitting of an individual into two or more individuals
budding	development of an outgrowth and then detachment of that outgrowth to form offspring
self-fertilization	zygote forms from fusion of sperm and egg from a single individual

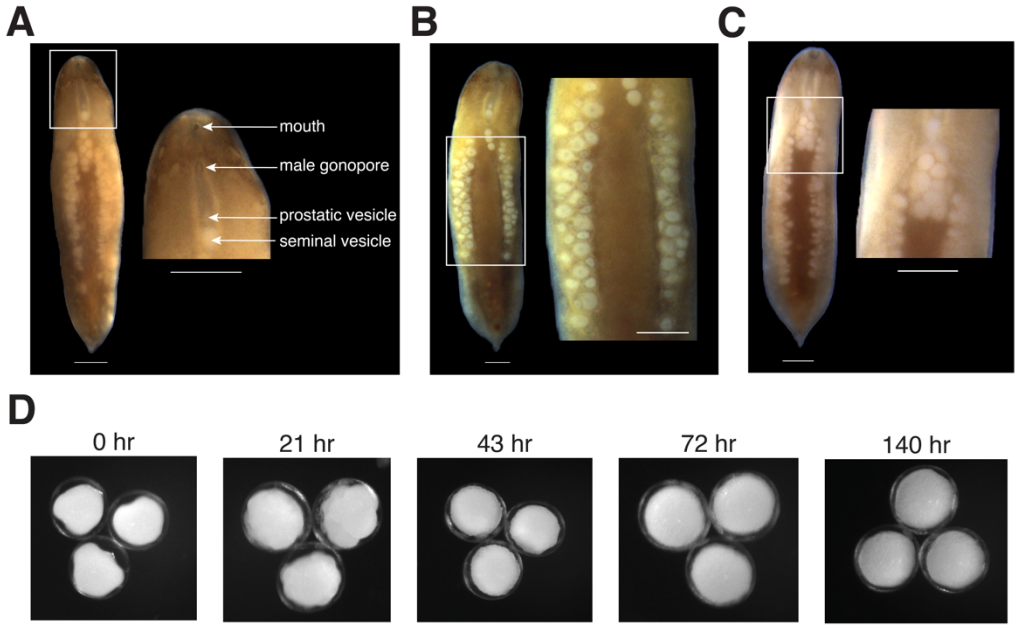

Figure S1: Gross reproductive morphology is visible from the ventral surface of *H. miamia*. (A) The male reproductive system includes the male gonopore, penis, prostatic vesicle, and seminal vesicle. (**B**) *H. miamia*'s ovaries are lateral, and organized along the anterior-posterior axis. There is no visible organization of oocytes by size or stage within the ovaries. (**C**) A cluster of zygotes is visible medially, and immediately posterior to the male copulatory apparatus. (**D**) Representative time course of embryonic development of embryos dissected from the central cavity. Scale bars: 1 mm.

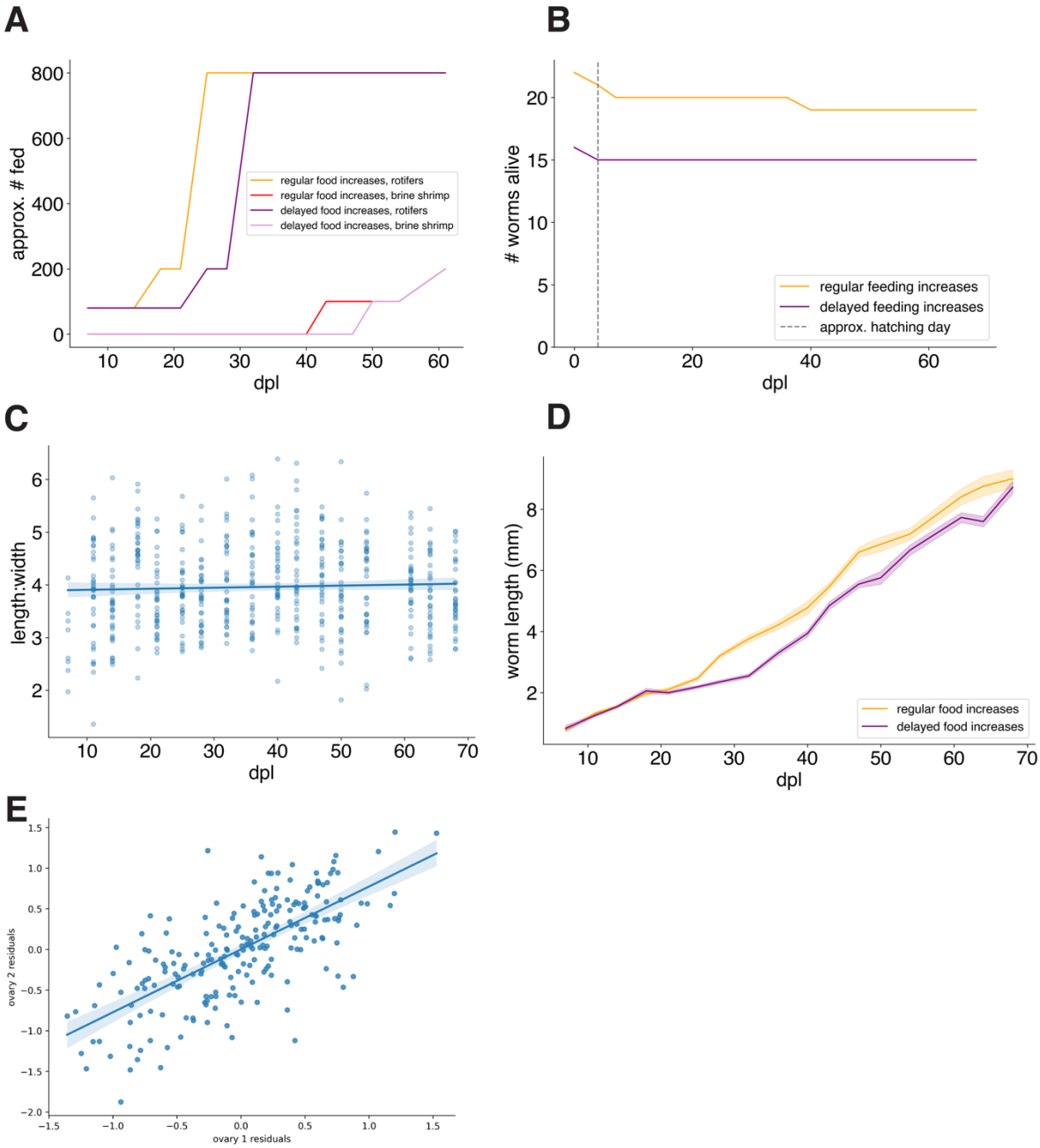

Figure S2: Growth and scaling. (**A**) Time course of feeding changes through juvenile development, showing the delayed increases in feeding for one group, and the introduction of brine shrimp late in development. (**B**) Survival curve showing the number of worms in each of the two feeding treatments over time. (**C**) The aspect ratio (length:width) of worms is consistent over time (slope = 0.002, R^2 = 0.002, p = 0.31), showing that worms grow proportionally over development. Error band shows 95% confidence

interval. (**D)** Worm length increases over time, with worms growing more slowly when their increased feeding was delayed. Error band shows SEM. (**E**) Residuals of ovary length (regressed against body length) within each worm are highly correlated (Pearson correlation coefficient = 0.7, $p < 0.0001$). Error band shows 95% confidence interval.

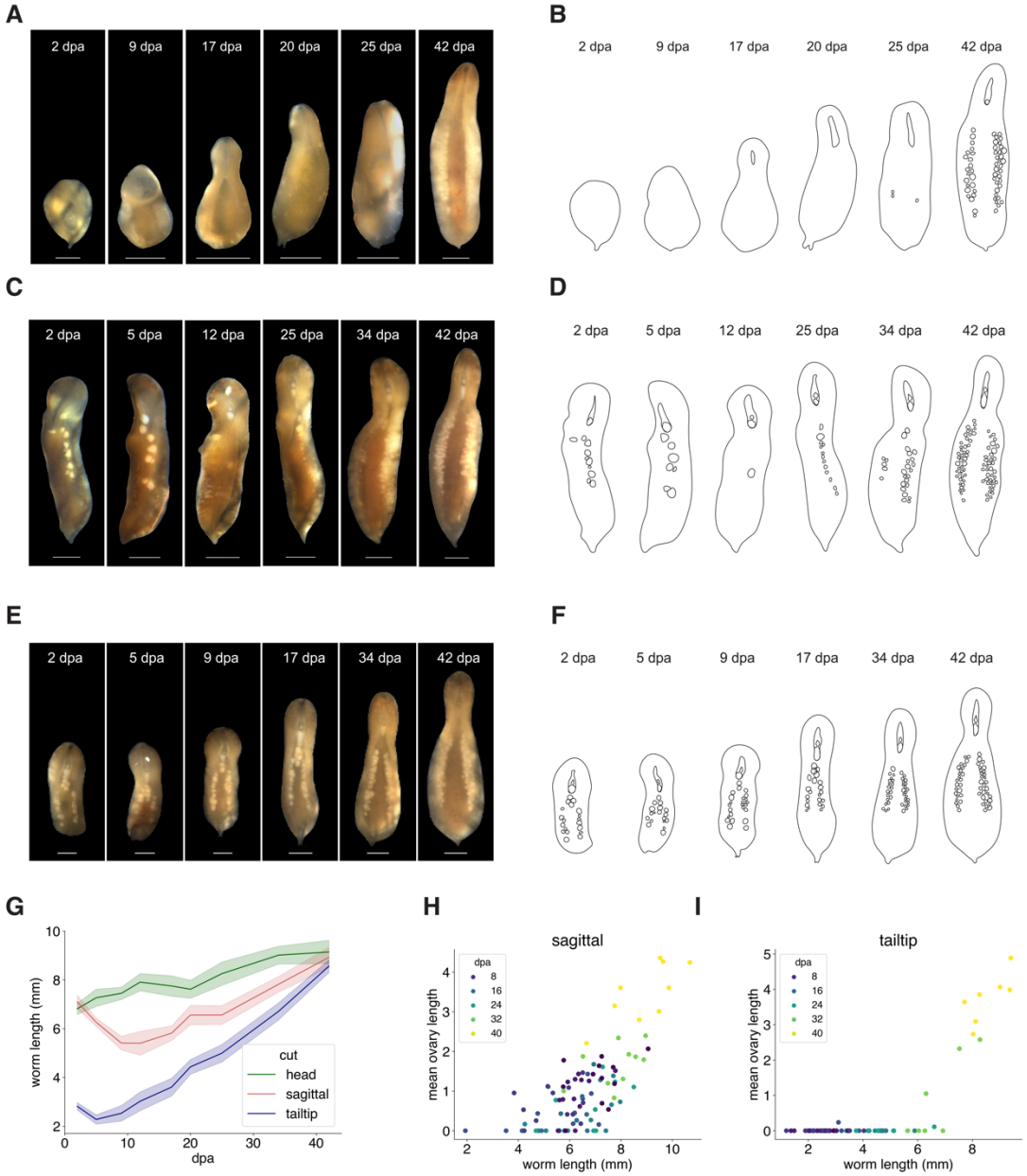

Figure S3: Across different growth contexts, body and organ scaling rules are conserved. (**A, C, E**) Representative time course of regenerating tail tip, sagittal cut, and head, and (**B, D, F**) schematized version with reproductive structures shown. (**G**) Regenerating heads and tail tips increase in length following amputation while sagittally-cut fragments shrink and then begin to grow. Error bar shows SEM. (**H**) Ovaries scale with body length in sagittally-cut fragments. (**I**) Ovaries regenerate once a tail fragment reaches a certain length. Scale bars: 1 mm.

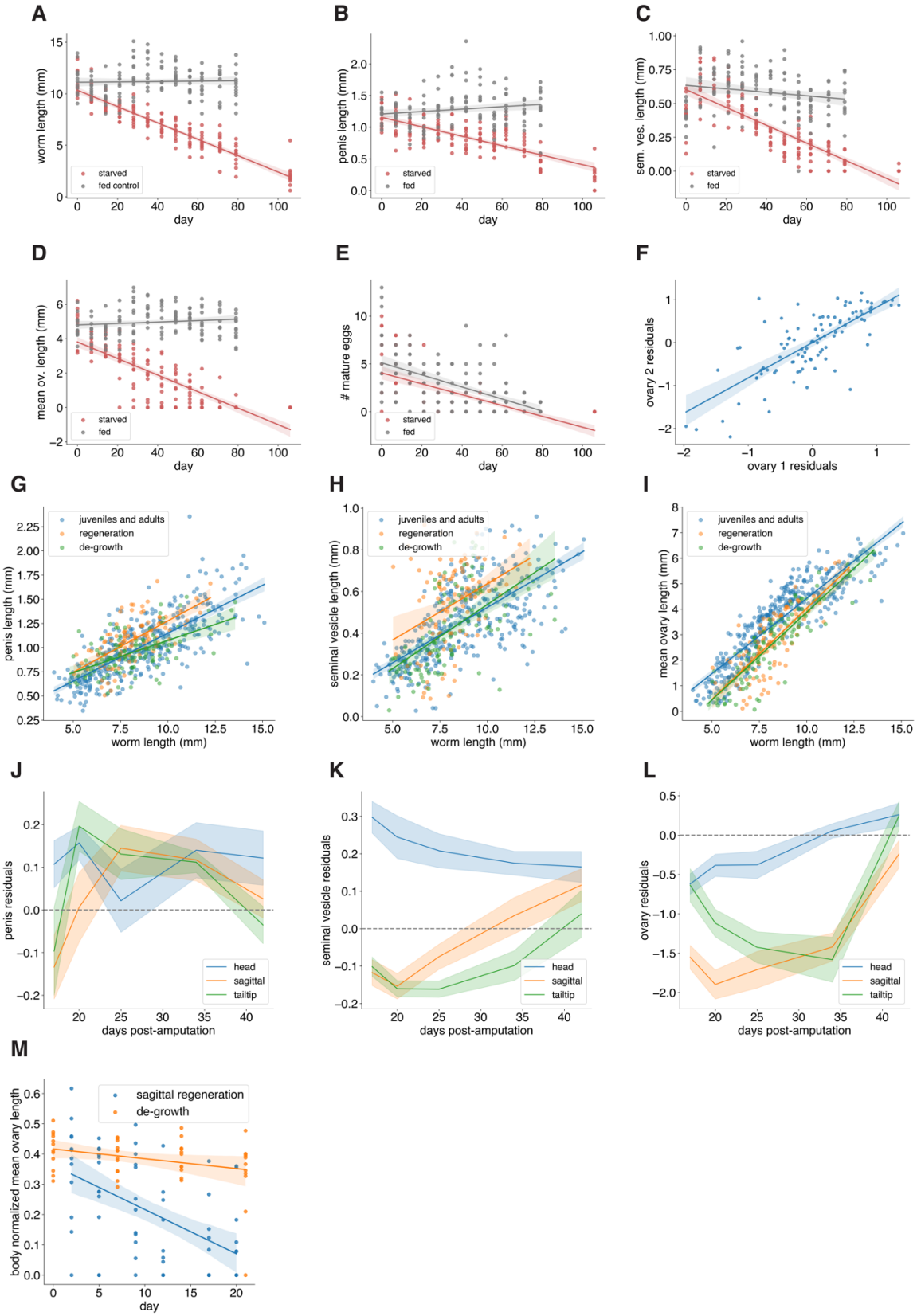
A
worm length (mm)
day
starved
fed control
B
penis length (mm)
day
starved
fed
C
sem. ves. length (mm)
day
starved
fed
D
mean ov. length (mm)
day
starved
fed
E
mature eggs
day
starved
fed
F
ovary 2 residuals
ovary 1 residuals
G
penis length (mm)
worm length (mm)
juveniles and adults
regeneration
de-growth
H
seminal vesicle length (mm)
worm length (mm)
juveniles and adults
regeneration
de-growth
I
mean ovary length (mm)
worm length (mm)
juveniles and adults
regeneration
de-growth
J
penis residuals
days post-amputation
head
sagittal
tailtip
K
seminal vesicle residuals
days post-amputation
head
sagittal
tailtip
L
ovary residuals
days post-amputation
head
sagittal
tailtip
M
body normalized mean ovary length
day
sagittal regeneration
de-growth

948

949 **Figure S4: Across different growth contexts, body and organ scaling rules are conserved.** (**A**)
950 Worm length decreases over time when worms are starved (starved: $R^2 = 0.85$, $p < 0.0001$; fed control:
951 $R^2 = 0.004$, $p = 0.48$). Error band shows 95% confidence interval. (**B-D**) Penis length (starved: $R^2 = 0.54$,
952 $p < 0.0001$; fed control: $R^2 = 0.04$, $p = 0.03$), seminal vesicle length (starved: $R^2 = 0.60$, $p < 0.0001$; fed
953 control: $R^2 = 0.03$, $p = 0.06$), and mean ovary length (starved: $R^2 = 0.67$, $p < 0.0001$; fed control: $R^2 =$
954 0.02, $p = 0.15$) decrease over time for worms experiencing de-growth but do not change in worms that
955 are continuously fed. Error band shows 95% confidence interval. (**E**) The number of zygotes in the central
956 cavity decreases over time in both starved and fed worms, likely because these worms are isolated
957 (starved: $R^2 = 0.48$, $p < 0.0001$; fed control: $R^2 = 0.33$, $p < 0.0001$). Error band shows 95% confidence
958 interval. (**F**) When controlling for the effect of body size, the residuals of ovary length (regressed against
959 body length) are strongly correlated between ovaries within worms over the course of de-growth (Pearson
960 correlation coefficient = 0.75, $p < 0.0001$). Error band shows 95% confidence interval. (**G-I**) The size of
961 reproductive structures scale similarly (see Table S3) across development, de-growth, and regeneration
962 (penis $R^2 = 0.70$, $p < 0.0001$; seminal vesicle: $R^2 = 0.50$, $p < 0.0001$; ovary: $R^2 = 0.76$, $p < 0.0001$). Error
963 band shows 95% confidence interval. **(J-L**) The residuals of organ length (regressed against body length)
964 generally converge towards zero over the course of regeneration despite sometimes displaying large
965 initial deviations. (**M**) Sagittal fragments degrade their existing ovary during initial regeneration at a faster
966 rate normalized to body size (slope = -0.015) than adult worms experiencing de-growth (slope = -0.003)
967 (Wald's test on slope of linear regression of ovary length and day: p=0.0006). Error band shows 95%
968 confidence interval.
969

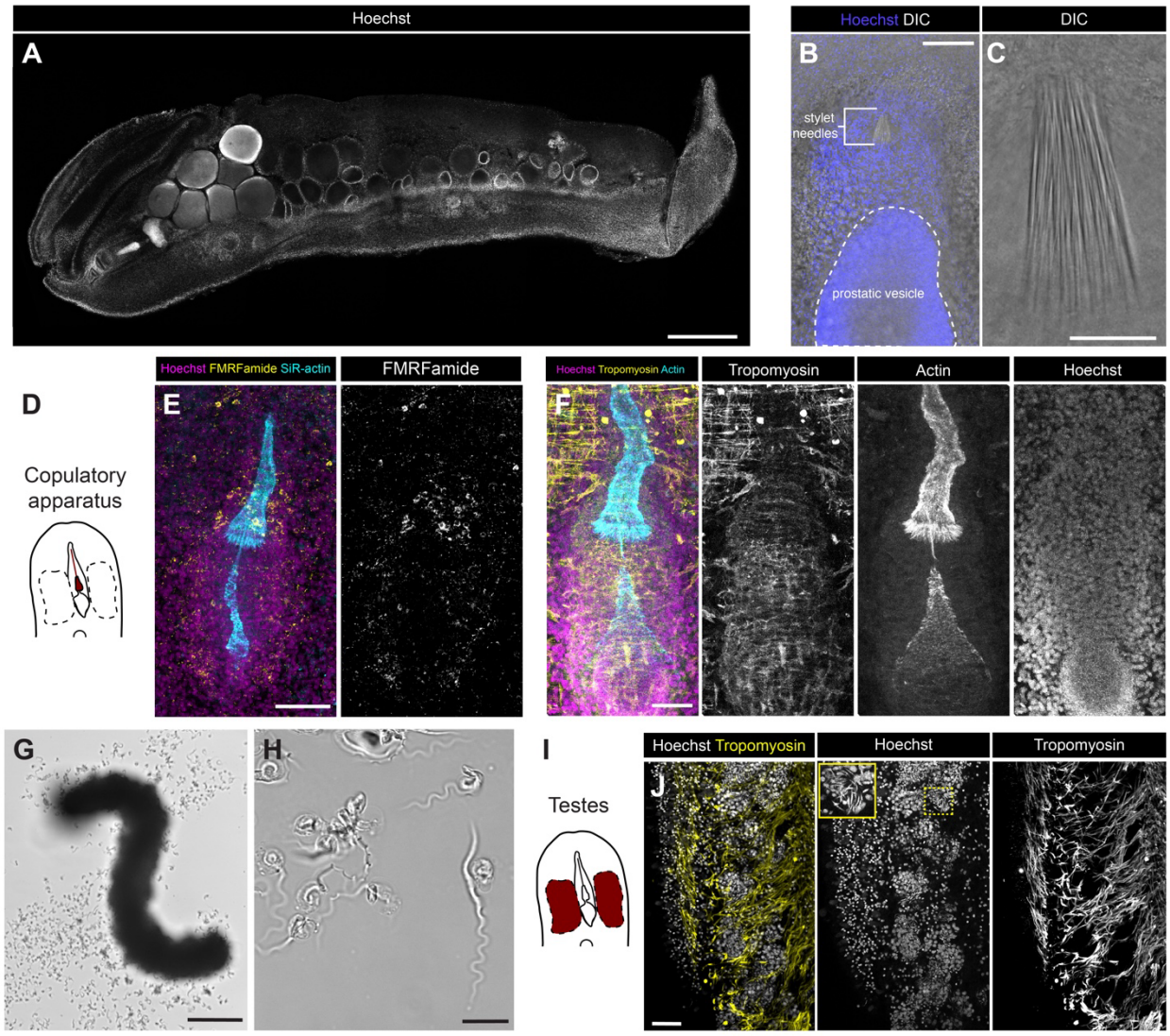

Figure S5: Fine structure of *H. miamia*'s male reproductive system. (**A**) The gross morphology and location of the reproductive system can be seen in sagittally-cut worms with nuclear staining. (**B-C**) Penis stylets are arranged in a bundle, seen with differential interference contrast (DIC). (**D**) Schematic of the male reproductive structures with the copulatory apparatus highlighted. (**E**) Antibody staining for FMRFamide shows that the penis sheath is surrounded by presumptive neurons. (**F**) Immunofluorescence for tropomyosin, and actin and nuclear labeling enables visualization of the musculature surrounding the male structures. (**G**) A packet of sperm ejected during mating made up of (**H**) sperm cells. (**I**) Schematic of the male reproductive structures with the testes highlighted. (**J**) Sperm in the testes develop in clusters interspersed with the muscle of the body, visualized by

immunofluorescence for tropomyosin, a muscle marker. Scale bars: 500μm (A), 100μm (B, G), 50μm (C, E, J), 25μm (F), 10μm (H).

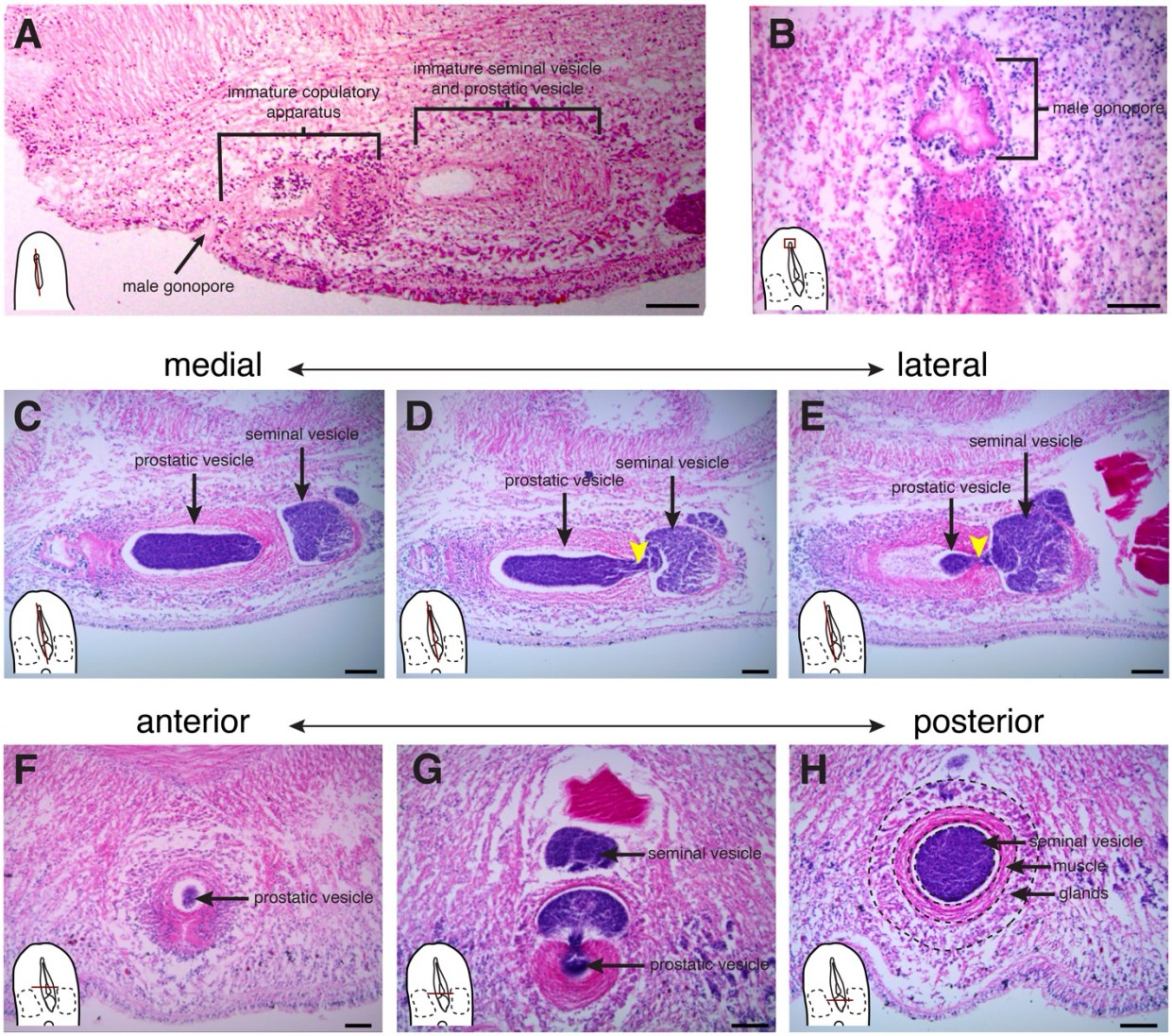

Figure S6: Histology of the male reproductive system reveals the organization of the male reproductive system along different body axes. (A) The male reproductive system in a sagittal section of a juvenile worm has a male gonopore but lacks a clear male copulatory apparatus, prostatic vesicle, and seminal vesicle. **(B)** A longitudinal section showing the male gonopore. **(C-E)** Sagittal sections through the male reproductive system along the medial-lateral axis showing a channel of sperm (yellow arrows) connecting the prostatic vesicle and seminal vesicle. **(F-H)** Transverse sections moving along the

990 anterior-posterior axis show the positions of the prostatic vesicle and seminal vesicle and the musculature

991 and glands surrounding the seminal vesicle. Scale bars: 100 um.

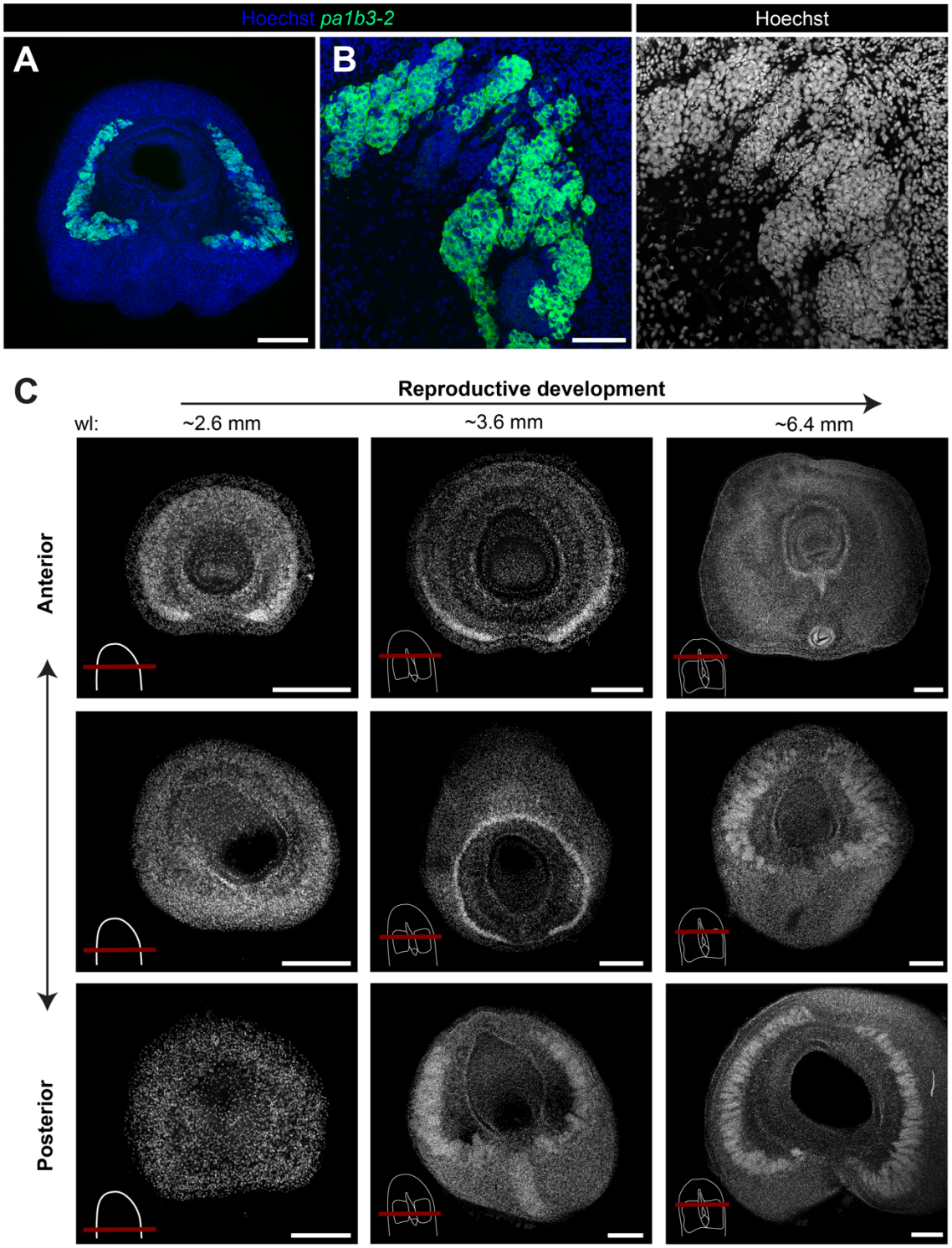

992

993 **Fig. S7: Testes emerge as lateralized regions and grow to span the dorsal surface as**
994 **worms grow.** (**A**) FISH for the male germline marker *pa1b3-2* results in two regions of
995 ventrolateral expression that extend toward the dorsal surfaces. (**B**) Hoechst and *pa1b3-2*
996 mRNA expression label sperm cells. (**C**) Nuclear staining of cross-sections at different points
997 along the anterior-posterior axis within the head shows that the testes emerge as two lateral
998 lobes that gradually form a continuous cylindrical structure. Cartoons depict the plane of
999 sectioning (red line) and reproductive structures (white). Scale bars: 250 µm (A), 50µm (B),
1000 200µm (C).
1001
1002

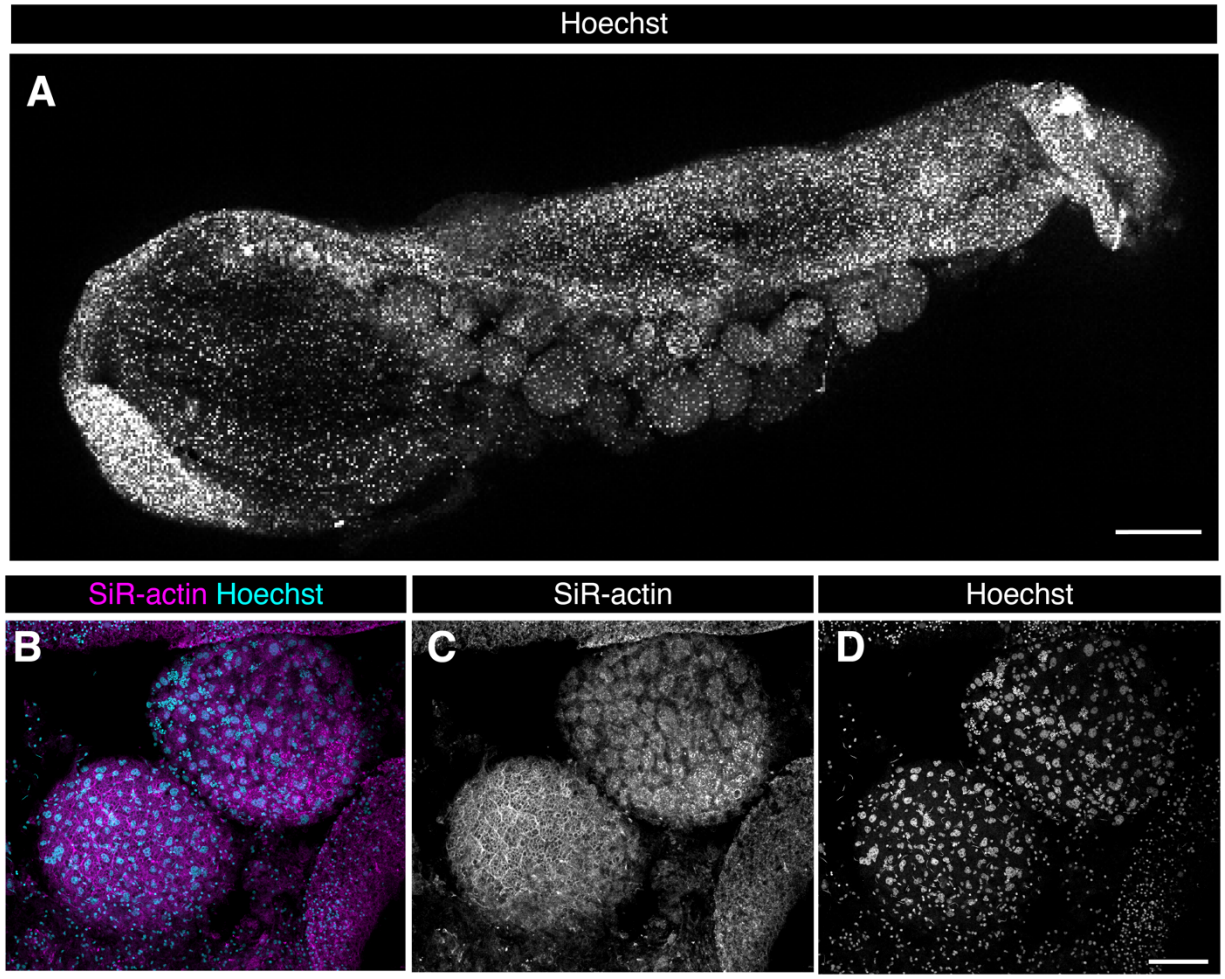

1003

Figure S8: Oocytes in *Hofstenia*'s ovaries are surrounded by follicular cells regardless of position or maturity. (**A**) Nuclear staining on a sagittal-cut worm confirms the presence of ovaries along the ventral side of the worm. Consistent with our other imaging, ovaries lack any sense of organization in regards to maturity along the anterior-posterior axis. (**B-D**) Oocytes are surrounded by a layer of follicular cells. Scale bars: 500µm (A), 100µm (D).

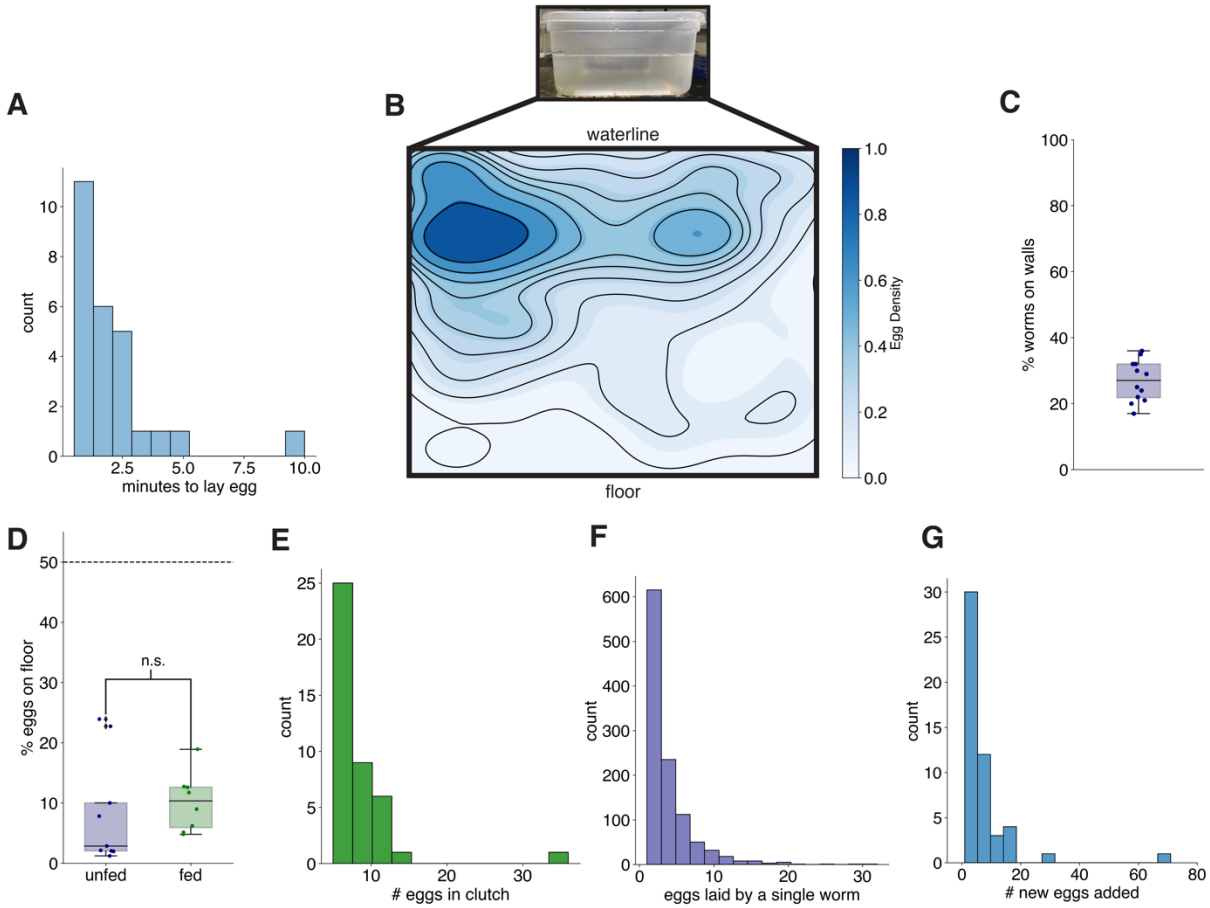

Figure S9: Worms have spatial preferences during egg-laying that are robust to suboptimal conditions. (**A**) Quantifying the time from the start of visible muscle contractions to egg laying reveals that the egg-laying process spans a timescale of seconds to minutes for each egg, with most eggs being laid within 3 minutes. (**B**) Kernel density estimate of egg locations on the short walls of the worm tanks (n = 1390 eggs). (**C**) Random observations of worms in their culture tanks (n = 12 tanks) finds only a minority of worms on the upper half of tank walls, even in conditions where we expect them to be actively

laying eggs. (**D**) Worms preferentially avoid laying eggs on the floor of the tank regardless of whether they are fed or unfed (two-sample t-test: $p= 0.62$, $n \geq 8$). (**E**) Distribution of clutch sizes in communal tanks ($n = 42$ clutches) shows that clutches frequently contain more than 10 eggs laid within a 3-4 day window. (**F**) Distribution of eggs laid by individual worms across different egg laying contexts shows that most worms lay fewer than 10 eggs in a 3-4 day window (**G**) Worms often add eggs to clutches constructed by other worms; the distribution shows the numbers of new eggs added to old clutches.

Video 1: The penis sheath is ciliated. Live-imaging of the ventral surface of a worm shows beating cilia lining the sheath. This set of cilia is distinct from the cilia lining the epidermis of the worm.

Video 2: The male gonopore is ciliated. Live imaging of the ventral surface of a worm shows that the male gonopore has beating cilia.

Video 3: Eggs are laid through the mouth. Video of an adult worm laying eggs, filmed from the ventral surface at 1Hz and sped up 2000x. The worm lowers its mouth and then contracts its body. During these contractions, a cluster of mature eggs can be seen distending the body. An individual egg is loaded into and travels through the pharynx eventually emerging through the mouth.

References

Abalde S, Jondelius U. 2024. A phylogenomic backbone for Acoelomorpha inferred from transcriptomic data. *Syst Biol*. doi:10.1093/sysbio/syae057

Achatz JG, Chiodin M, Salvenmoser W, Tyler S, Martinez P. 2013. The Acoela: on their kind and kinships, especially with nemertodermatids and xenoturbellids (Bilateria incertae sedis). *Org Divers Evol* **13**:267–286.

Achatz JG, Hooge MD. 2006. Convolutidae (Acoela) from Tanzania. *Zootaxa* **1362**:1.

Ahyong S, Boyko CB, Bernot J, Brandão SN, Daly M, De Grave S, de Voogd NJ, Gofas S, Hernandez F, Hughes L, Neubauer TA, Paulay G, van der Meij S, Boydens B, Decock W, Dekeyzer S, Goharimanesh M, Vandepitte L, Vanhoorne B, Adlard R, Agatha S, Ahn KJ, Alonso MV, Alvarez B, Amler MRW, Amorim V, Anderberg A, Andrés-Sánchez S, Ang Y, Antić D, Antonietto LS, Arango C, Artois T, Atkinson S, Auffenberg K, Bailly N, Baldwin BG, Bank R, Barber A, Barrett RL, Bartsch I, Bellan-Santini D, Bergh N, Bernard C, Berrios Ortega FJ, Berta A, Bezerra TN, Bieler R, Blanco S, Blasco-Costa I, Blazewicz M, Błędzki LA, Bock P, Bonifacino M, Böttger-Schnack R, Bouchet P, Boury-Esnault N, Bouzan R, Boxshall G, Bray R, Brito Seixas AL, Bruce NL, Bruneau A, Budaeva N, Bueno-Villegas J, Calvo Casas J, Cárdenas P, Carstens E, Cartwright P, Cedhagen T, Chan BK, Chan TY, Chernyshev A, Choong H, Christenhusz M, Churchill M, Collins AG, Collins GE, Collins K, Consorti L, Copilaș-Ciocianu D, Corbari L, Cordeiro R, Costa VM d. M, Costa Corgosinho PH, Coste M, Costello MJ, Crandall KA, Cremonte F, Cribb T, Cuscó-Borràs J, Cutmore S, Dahdouh-Guebas F, Daneliya M, Dauvin JC, Davie P, De Broyer C, de Lima Ferreira P, de Mazancourt V, de Moura Oliveira L, Decker P, Defaye D, Dekker H, Di Capua I, Dippenaar S, Dohrmann M, Dolan J, Domning D, Downey R, Dreyer N, Eisendle U, Eitel M, Eleaume M, Enghoff H, Epler J, Esquete Garrote P, Evenhuis NL, Ewers-Saucedo C, Faber M, Figueroa D, Fišer C, Fordyce E, Foster W, Fransen C, Freire S, Fujimoto S, Furuya H, Galán-Díaz J, Galbany-Casals M, Gale A, Galea H, Gao T, García-Moro P, Garic R, Garnett S, Gaviria-Melo S, Gerken S, Gibson D, Gibson R, Gil J, Gittenberger A, Glasby C, Glenner H, Glover A, Gómez I, Gómez-Noguera SE, Gondim AI, Gonzalez BC, González-Solís D, Goodwin C, Gostel M, Grabowski M, Gravili C, Grossi M, Guerra-García JM, Guerrero JM, Guidetti R, Guiry, Gutierrez D, Hadfield KA, Hajdu E, Halanych K, Hallermann J, Hayward BW, Hegna TA, Heiden G, Hendrycks E, Hennen D, Herbert D, Herrera Bachiller A, Hodda M, Høeg J, Hoeksema B, Holovachov O, Hooge, Hooper JN, Horton T, Houart R, Huys R, Hyžný M, Iniesta LFM, Iseto T, Iwataki M, Janssen R, Jaume D, Jazdzewski K, Jersabek CD, Jiménez-Mejías P, Jóźwiak P, Kabat A, Kajihara H, Kakui K, Kantor Y, Karanovic I, Karapunar B, Karthick B, Kathirithamby J, Katinas L, Kilian N, Kim YH, King R, Kirk PM, Klautau M, Kociolek JP, Köhler F, Konowalik K, Kotov A, Kovács Z, Kremenetskaia A, Kristensen RM, Kroh A, Kulikovskiy M, Kullander S, Kupriyanova E, Lamaro A, Lambert G, Larridon I, Lazarus D, Le Coze F, Le Roux M, LeCroy S, Leduc D, Lefkowitz EJ, Lemaitre R, Lichter-Marck IH, Lim SC, Lindsay D, Liu Y, Loeuille B, Lois R, Lörz AN, Ludwig T, Lundholm N, Macpherson E, Maguilla E, Mah C, Mamos T, Manconi R, Mapstone G, Marek PE, Markello K, Márquez-Corro JI, Marshall B, Marshall DJ, Martin P, Martín-Bravo S, Martinez Arbizu P, Maslakova S, McFadden C, McInnes SJ, McKenzie R, Means J, Mees J, Mejía-Madrid HH, Meland K, Merrin KL, Míguez M, Miller J, Mills C,

Moestrup Ø, Mokievsky V, Molodtsova T, Monniot F, Mooi R, Morales-Alonso A, Morandini AC, Moreira da Rocha R, Morrow C, Mortelmans J, Müller A, Muñoz Gallego AR, Muñoz Schüler P, Musco L, Nascimento JB, Nesom G, Neto Silva M d. S, Neubert E, Neuhaus B, Ng P, Nguyen AD, Nielsen C, Nielsen S, Nishikawa T, Norenburg J, O'Hara T, Opresko D, Osawa M, Osigus HJ, Ota Y, Páll-Gergely B, Panero JL, Patterson D, Pedram M, Pelser P, Peña Santiago R, Perbiche-Neves G, Pereira J d. S, Pereira PHM, Pereira SGG, Perez-Losada M, Petrescu I, Pfingstl T, Piasecki W, Pica D, Picton B, Pignatti J, Pilger JF, Pinheiro U, Pisera AB, Poatskievick Pierezan B, Polhemus D, Poore GC, Potapova M, Praxedes RA, Půža V, Read G, Reich M, Reimer JD, Reip H, Resende Bueno V, Reuscher M, Reynolds JW, Richling I, Rimet F, Ríos P, Rius M, Rodríguez E, Rogers DC, Roque N, Rosenberg G, Rützler K, Sa IR d. S, Sá HAB, Saavedra M, Sabater LM, Sabbe K, Sabroux R, Saiz-Salinas J, Sala S, Samimi-Namin K, Sánchez-Villegas M, Sánchez-Villegas R, Santagata S, Santos S, Santos SG, Santos Filho MAB d., Sanz Arnal M, Sar E, Saucède T, Schärer L, Schierwater B, Schilling E, Schmidt-Lebuhn A, Schneider S, Schönberg C, Schrével J, Schuchert P, Schweitzer C, Semple JC, Senna AR, Sennikov A, Serejo C, Shaik S, Shamsi S, Sharma J, Shear WA, Shenkar N, Short M, Sicinski J, Sierwald P, Silva DKF d., Silva ESS, Silva MLCN, Simmons E, Sinniger F, Sinou C, Sivell D, Smit H, Smit N, Smol N, Sørensen MV, Souza-Filho JF, Spelda J, Sterrer W, Steyn HM, Stoev P, Stöhr S, Suárez-Morales E, Susanna A, Suttle C, Swalla BJ, Taiti S, Tanaka M, Tandberg AH, Tang D, Tasker M, Taylor J, Taylor J, Taylor K, Tchesunov A, Temereva E, ten Hove H, ter Poorten JJ, Thirouin K, Thomas JD, Thuesen EV, Thurston M, Thuy B, Timi JT, Todaro A, Todd J, Turon X, Tyler S, Uetz P, Urbatsch L, Uribe-Palomino J, Urtubey E, Utevsky S, Vacelet J, Vader W, Väinölä R, Valdés-Florido A, Valls Domedel G, Van de Vijver B, van Haaren T, van Soest RW, Vanreusel A, Vázquez-García B, Velandia J, Venekey V, Verhoeff T, Villaverde T, Vinarski M, Vonk R, Vos C, Vouilloud AA, Walker-Smith G, Walter TC, Watling L, Wayland M, Wesener T, Wetzel CE, Whipps C, White K, Wieneke U, Williams DM, Williams G, Williams N, Wilson KL, Wilson R, Witkowski J, Wyatt N, Xavier J, Xu K, Zanol J, Zeidler W, Zhao Z, Zullini A. 2024. World Register of Marine Species.

Åkesson B, Gschwentner R, Hendelberg J, Ladurner P, Müller J, Rieger R. 2001. Fission in Convolutriloba longifissura: asexual reproduction in acoelous turbellarians revisited. *Acta Zool* **82**:231–239.

Allard P, Tabin CJ. 2009. Achieving bilateral symmetry during vertebrate limb development. *Semin Cell Dev Biol* **20**:479–484.

Apelt G. 1969. Fortpflanzungsbiologie, Entwicklungszyklen und vergleichende Frühentwicklung acoeler Turbellarien. *Mar Biol* **4**:267–325.

Ax P, Schulz E. 1959. Ungeschlechtliche Fortpflanzung durch Paratomie bei acoelen Turbellarien. *Biol Zent Bl* **78**:613–622.

Bailly X, Laguerre L, Correc G, Dupont S, Kurth T, Pfannkuchen A, Entzeroth R, Probert I, Vinogradov S, Lechauve C, Garet-Delmas M-J, Reichert H, Hartenstein V. 2014. The chimerical and multifaceted marine acoel Symsagittifera roscoffensis: from photosymbiosis to brain regeneration. *Front Microbiol* **5**. doi:10.3389/fmicb.2014.00498

Ballarin L, Burighel P, Cima F. 2008. A tale of death and life: natural apoptosis in the colonial ascidian Botryllus schlosseri (Urochordata, Ascidiacea). *Curr Pharm Des* **14**:138–147.

Beltagi S, Mandura A. 1991. Hofstenia arabiensis Nov. Sp. (Hofsteniidae): A New Species of Acoelan Turbellaria from the Red Sea North of Jeddah. *Journal of King Abdulaziz University-science* **3**:65–90.

Bock S. 1923. Eine neue marine Turbellariengattung aus Japan. Almqvist & Wiksell.

Boone M, Houthoofd W, Bert W, Artois T. 2011. First record of Nemertodermatida from Belgian marine waters. *Belg J Zool* **141**:62–64.

Boulan L, Léopold P. 2021. What determines organ size during development and regeneration? *Development* **148**:dev196063.

Brand JN, Harmon LJ, Schärer L. 2022a. Frequent origins of traumatic insemination involve convergent shifts in sperm and genital morphology. *Evolution Letters* **6**:63–82.
Brand JN, Harmon LJ, Schärer L. 2022b. Mating behavior and reproductive morphology predict macroevolution of sex allocation in hermaphroditic flatworms. *BMC Biol* **20**:35.
Brand JN, Viktorin G, Wiberg RAW, Beisel C, Schärer L. 2022c. Large-scale phylogenomics of the genus Macrostomum (Platyhelminthes) reveals cryptic diversity and novel sexual traits. *Mol Phylogenet Evol* **166**:107296.
Bush L. 1975. Biology of Neochilda fusca N. gen., n. sp. from the northeastern coast of the United States (Platyhelminthes: Turbellaria). *Biol Bull* **148**:35–48.
Cannon JT, Vellutini BC, Smith J, Ronquist F, Jondelius U, Hejnol A. 2016. Xenacoelomorpha is the sister group to Nephrozoa. *Nature* **530**:89–93.
Charnov EL. 1979. Simultaneous hermaphroditism and sexual selection. *Proc Natl Acad Sci U S A* **76**:2480–2484.
Chiodin M, Børve A, Berezikov E, Ladurner P, Martinez P, Hejnol A. 2013. Mesodermal gene expression in the acoel Isodiametra pulchra indicates a low number of mesodermal cell types and the endomesodermal origin of the gonads. *PLoS One* **8**:e55499.
Corrêa DD. 1960. Two New Marine Turbellaria from Florida. *Bull Mar Sci* **10**:208–216.
Costello HM, Costello DP. 1939. EGG LAYING IN THE ACOELOUS TURBELLARIAN POLYCHOERUS CARMELENSIS. *Biol Bull* **76**:80–89.
Costello HM, Costello DP. 1938. COPULATION IN THE ACŒLOUS TURBELLARIAN POLYCHŒRUS CARMELENSIS. *Biol Bull* **75**:85–98.
Crezee M. 1978. Paratomella rubra Rieger and Ott, an amphiatlantic acoel turbellarian. *Cah Biol Mar* **19**:1–9.
Crezée M. 1975. Monograph of the solenofilomorphidae (Turbellaria: Acoela). *Int Rev Gesamt Hydrobiol* **60**:769–845.
Davies N, Krebs J, West S. 2013. An Introduction to Behavioural Ecology. Wiley-Blackwell.
De Mulder K, Kuales G, Pfister D, Willems M, Egger B, Salvenmoser W, Thaler M, Gorny A-K, Hrouda M, Borgonie G, Ladurner P. 2009. Characterization of the stem cell system of the acoel Isodiametra pulchra. *BMC Dev Biol* **9**:69.
Dörjes J. 1968. Die Acoela (Turbellaria) der Deutschen Nordseeküste und ein neues System der Ordnung. *J Zoolog Syst Evol Res* **6**:56–452.
Dörjes J. 1966. Paratomella unichaeta, nov. gen. nov. spec., Vertreter einen neuen Familie der Turbellaria Acoela mit asexueller Fortpflanzung durch Paratomie. *Veröffentlichungen des Instituts für Meeresforschung in Bremerhaven* **II**:187–200.
du Bois-Reymond Marcus E. 1955. On Turbellaria and Polygordius from the Brazilian Coast. *Bol Fac Fil Ci Letr Univ Sao Paulo Zool* **20**:19–53.
Eckelbarger K, Hodgson A. 2021. Invertebrate oogenesis – a review and synthesis: comparative ovarian morphology, accessory cell function and the origins of yolk precursors. *Invertebr Reprod Dev* **65**:71–140.
Falleni A, Gremigni V. 1990. Ultrastructural study of oogenesis in the acoel turbellarian Convoluta. *Tissue Cell* **22**:301–310.
Faubel A. 1983. The Polycladida, Turbellaria. Proposal and establishment of a new system. Part I. The Acotylea. *Mitt Hamb Zool Mus Inst* **80**:17–121.
Faubel A. 1976. Interstitielle Acoela (Turbellaria) aus dem Littoral der nordfriesischen Inseln Sylt und Amrum. *Mitt Hamb Zool Mus Inst* **73**:17–56.
Faubel A. 1974. Die Acoela (Turbellaria) eines Sandstrandes der Nordseeinsel Sylt. *Mikrofauna Meeresbodens* **32**:1–58.
Faubel A, Cameron B. 2001. Platyhelminthes from salt marshes of Coomera River, Southeastern Queensland, Australia. *Mem Queensland Mus* **46**:511–519.
Gardiner E. 1898. The Growth of the Ovum, Formation of the Polar Bodies, and the Fertilization in Polychaerus Caudatus.

1191 Gardiner E. 1895. Early development of Polychoerus Caudatus, Mark. *J Morphol* **11**:155–176.
1192 Gehrke AR, Neverett E, Luo Y-J, Brandt A, Ricci L, Hulett RE, Gompers A, Ruby JG, Rokhsar
1193 DS, Reddien PW, Srivastava M. 2019. Acoel genome reveals the regulatory landscape of
1194 whole-body regeneration. *Science* **363**:eaau6173.
1195 Giribet G, Edgecombe GD. 2020. The Invertebrate Tree of Life. Princeton University Press.
1196 Grae D, Kozloff E. 1999. Post-copulatory storage of sperm in the seminal bursa of the acoel
1197 flatworm Otocelis luteola. *Invertebr Reprod Dev* **35**:151–154.
1198 Grossman H, Har-Paz E, Gindi N, Levi M, Miller I, Nevo N, Galiani D, Dekel N, Shalgi R. 2017.
1199 Regulation of GVBD in mouse oocytes by miR-125a-3p and Fyn kinase through modulation
1200 of actin filaments. *Sci Rep* **7**:2238.
1201 Hanson ED. 1960. Asexual Reproduction in Acoelous Turbellaria. *Yale J Biol Med* **33**:107–111.
1202 Harris MP, Daane JM, Lanni J. 2021. Through veiled mirrors: Fish fins giving insight into size
1203 regulation. *Wiley Interdiscip Rev Dev Biol* **10**:e381.
1204 Herlands L, Maul GG. 1994. Characterization of a major nucleoplasmin-like germinal vesicle
1205 protein which is rapidly phosphorylated before germinal vesicle breakdown in Spisula
1206 solidissima. *Dev Biol* **161**:530–537.
1207 Hooge M. 2003. Two new families, three new genera, and five new species of acoels (Acoela
1208 Platyhelminthes) from Queensland Australia. *Cah Biol Mar* **44**:275–298.
1209 Hooge M, Smith JPS. 2004. New acoels (Acoela, Acoelomorpha) from North Carolina. *Zootaxa*
1210 **442**:1–24.
1211 Hooge M, Wallberg A, Todt C, Maloy A, Jondelius U, Tyler S. 2007. A revision of the
1212 systematics of panther worms (Hofstenia spp., Acoela), with notes on color variation and
1213 genetic variation within the genus. *Hydrobiologia* **592**:439–454.
1214 Hookabe N, Jimi N, Furushima Y, Fujiwara Y. 2024. Discovery of deep-sea acoels from a
1215 chemosynthesis-based ecosystem. *Biol Lett* **20**:20230573.
1216 Hulett RE, Kimura JO, Bolaños DM, Luo Y-J, Rivera-López C, Ricci L, Srivastava M. 2023.
1217 Acoel single-cell atlas reveals expression dynamics and heterogeneity of adult pluripotent
1218 stem cells. *Nat Commun* **14**:2612.
1219 Hulett RE, Potter D, Srivastava M. 2020. Neural architecture and regeneration in the acoel
1220 Hofstenia miamia. *Proceedings of the Royal Society B: Biological Sciences* **287**:20201198.
1221 Hyman LH. 1951. The invertebrates: Platyhelminthes and Rhynchocoela. The acoelomate
1222 Bilateria. McGraw-Hill, New York.
1223 Hyman LH. 1937. Reproductive system and copulation in amphiscolops langerhansi (turbellaria
1224 acoela). *Biol Bull* **72**:319–326.
1225 Ishikawa K, Yamasu T. 1992. An acoel flat worm species related closely to the species
1226 Convolutriloba retrogemma Hendelberg and Akesson occurs in Okinawa Island, Ryukyu
1227 Archipelago. *Zoological Science* **9**:1281.
1228 Jondelius U, Wallberg A, Hooge M, Raikova OI. 2011. How the Worm Got its Pharynx:
1229 Phylogeny, Classification and Bayesian Assessment of Character Evolution in Acoela. *Syst*
1230 *Biol* **60**:845–871.
1231 Kapli P, Telford MJ. 2020. Topology-dependent asymmetry in systematic errors affects
1232 phylogenetic placement of Ctenophora and Xenacoelomorpha. *Sci Adv* **6**:eabc5162.
1233 Kimura JO, Bolaños DM, Ricci L, Srivastava M. 2022. Embryonic origins of adult pluripotent
1234 stem cells. *Cell* **185**:4756–4769.e13.
1235 Kimura JO, Ricci L, Srivastava M. 2021. Embryonic development in the acoel Hofstenia miamia.
1236 *Development* **148**:dev188656.
1237 Ko JM, Reginato W, Wolff A, Lobo D. 2024. Mechanistic regulation of planarian shape during
1238 growth and degrowth. *Development* **151**:dev202353.
1239 Kostenko AG. 1989. The position of Taurida fulvomaculata (Ax, 1959) in the system of Acoela.
1240 In: Morphology of turbellarians. *Akad Nauk USSR Trudy Zool* **195**:14–25.
1241 Kozloff EN. 2000a. Differentiation, dedifferentiation, and redifferentiation of reproductive

structures of the acoel flatworm*Otocelis luteola*, and notes on longevity of this species. *Invertebr Reprod Dev* **37**:95–106.
Kozloff EN. 2000b. A new genus and five new species of acoel flatworms from the Pacific coast of North America, and resolution of some systematic problems in the families Convolutidae and Otocelididae. *Cah Biol Mar* **41**:281–293.
Liu J-L, Buszczak M, Gall JG. 2006. Nuclear bodies in the Drosophila germinal vesicle. *Chromosome Res* **14**:465–475.
Mamkaev YV. 1965. Etude morphologique d'Actinoposthia beklemischevi n. sp. (Turbellaria Acoela). *Cah Biol Mar* **6**:23–50.
Meyer-Wachsmuth I, Curini Galletti M, Jondelius U. 2014. Hyper-cryptic marine meiofauna: species complexes in Nemertodermatida. *PLoS One* **9**:e107688.
Michiels NK, Newman LJ. 1998. Sex and violence in hermaphrodites. *Nature* **391**:647–647.
Munro C, Cadis H, Pagnotta S, Houliston E, Huynh J-R. 2023. Conserved meiotic mechanisms in the cnidarian *Clytia hemisphaerica* revealed by *Spo11* knockout. *Sci Adv* **9**:eadd2873.
Peebles F. 1915. A Description of three Acoela from the Gulf of Naples. *Mitteilungen a.d Zool Station zu Neapel* **22**:292–312.
Pellettieri J, Fitzgerald P, Watanabe S, Mancuso J, Green DR, Sánchez Alvarado A. 2010. Cell death and tissue remodeling in planarian regeneration. *Dev Biol* **338**:76–85.
Perea-Atienza E, Botta M, Salvenmoser W, Gschwentner R, Egger B, Kristof A, Martinez P, Achatz JG. 2013. Posterior regeneration in Isodiametra pulchra (Acoela, Acoelomorpha). *Front Zool* **10**:64.
Petrov A, Hooge M, Tyler S. 2004. Ultrastructure of sperms in Acoela (Acoelomorpha) and its concordance with molecular systematics. *Invertebr Biol* **123**:183–197.
Philippe H, Brinkmann H, Copley RR, Moroz LL, Nakano H, Poustka AJ, Wallberg A, Peterson KJ, Telford MJ. 2011. Acoelomorph flatworms are deuterostomes related to Xenoturbella. *Nature* **470**:255–258.
Raikova O, Falleni A, Gremigni V. 1995. Oogenesis in Actinoposthia beklemischevi (Platyhelminthes, Acoela): an ultrastructural and cytochemical study. *Tissue Cell* **27**:621–633.
Ramm SA, Schlatter A, Poirier M, Schärer L. 2015. Hypodermic self-insemination as a reproductive assurance strategy. *Proceedings of the Royal Society B: Biological Sciences* **282**:20150660.
Reddien PW. 2018. The cellular and molecular basis for planarian regeneration. *Cell* **175**:327–345.
Ricci L, Srivastava M. 2021. Transgenesis in the acoel worm Hofstenia miamia. *Dev Cell* **56**:3160–3170.e4.
Rieger RM, Tyler S, Smith JPS, Rieger GE. 1991. Platyhelminthes and NemertineaMicroscopic Anatomy of Invertebrates. New York: Wiley-Liss. pp. 7–140.
Riser NW. 1987. Nemertinoides elongatus gen. n., sp. n. (Turbellaria: Nemertodermatida) from coarse sand beaches of the Western North Atlantic. *Proc Helminthol Soc Wash* **54**:60–67.
Rychel AL, Swalla BJ. 2008. Anterior regeneration in the hemichordate Ptychodera flava. *Dev Dyn* **237**:3222–3232.
Sagata N. 1996. Meiotic metaphase arrest in animal oocytes: its mechanisms and biological significance. *Trends Cell Biol* **6**:22–28.
Schärer L, Janicke T, Ramm SA. 2014. Sexual conflict in hermaphrodites. *Cold Spring Harb Perspect Biol* **7**:a017673.
Schärer L, Littlewood DTJ, Waeschenbach A, Yoshida W, Vizoso DB. 2011. Mating behavior and the evolution of sperm design. *Proceedings of the National Academy of Sciences* **108**:1490–1495.
Schmidt-Rhaesa A. 2007. The Evolution of Organ Systems. OUP Oxford.
Shannon T, Achatz J. 2007. Convolutriloba macropyga sp. nov., an uncommonly fecund acoel

(Acoelomorpha) discovered in tropical aquaria. *Zootaxa* **1525**:1–17.
Srivastava M. 2022. Studying development, regeneration, stem cells, and more in the acoel Hofstenia miamia. *Curr Top Dev Biol* **147**:153–172.
Srivastava M, Mazza-Curll KL, van Wolfswinkel JC, Reddien PW. 2014. Whole-Body Acoel Regeneration Is Controlled by Wnt and Bmp-Admp Signaling. *Curr Biol* **24**:1107–1113.
Steinböck O. 1966. Grundsätzliches zur Evolution der Turbellarien. *Zeitschrift für Zoologische Systematik und Evolutionsforschung* **4**:58–195.
Sterrer WE. 1998. New and known Nemertodermatida (Platyhelminthes- Acoelomorpha) - a revision. *Belgian Journal of Zoology* **128**:55–92.
Tong SJW, Ong RSL. 2020. Mating behavior, spawning, parental care, and embryonic development of some marine pseudocerotid flatworms (Platyhelminthes: Rhabditophora: Polycladida) in Singapore. *Invertebr Biol* **139**:e12293.
Trible W, Kronauer DJC. 2017. Caste development and evolution in ants: it's all about size. *J Exp Biol* **220**:53–62.
Tyler, S., Schilling, S., Hooge, M., & Bush, L. F. 2012. Turbellarian taxonomic database. Version 1.7. http://turbellaria.umaine.edu
Uppaluri S, Brangwynne CP. 2015. A size threshold governs Caenorhabditis elegans developmental progression. *Proc R Soc B* **282**:20151283.
Vallejo DM, Juarez-Carreño S, Bolivar J, Morante J, Dominguez M. 2015. A brain circuit that synchronizes growth and maturation revealed through Dilp8 binding to Lgr3. *Science* **350**:aac6767.
Wallberg A. 2012. The Stylet - Diversity and Systematics of Acoela and Nemertodermatida. http://acoela.myspecies.info
Watzin MC. 1984. Egg Laying in the Acoel Turbellarian Neochildia fusca. *Trans Am Microsc Soc* **103**:322–325.
Wolpert L. 2010. Arms and the man: the problem of symmetric growth. *PLoS Biol* **8**:e1000477.
Zabotin YI, Evtugyn VG. 2021. Ultrastructure of spermatozoa and female copulatory organs in preferably asexually-reproducing acoel Convolutriloba retrogemma (Acoelomorpha). *Zoomorphology* **140**:19–26.
Zauchner T, Salvenmoser W, Egger B. 2015. A cultivable acoel species from the Mediterranean, Aphanostoma pisae sp. nov. (Acoela, Acoelomorpha). *Zootaxa* **3941**:401–413.